Genome Biology

RESEARCH Open Access

Deciphering functional landscapes of rumen microbiota unveils the role of Prevotella bryantii in milk fat synthesis in goats

Yu Lei[1†], Yining Zheng[1†], Yiting Yan[1†], Kai Zhang[1], Xuyang Sun[1], Bo Yang[2], Lan Ge[1], Zhongming Meng[1], Xi Cao[1], Xiumin Zhang[3], Xiaoting Yan[4], Yangbin Xu[1], Ting Zhang[1], Jinping Shi[5], Shiwei Chen[6], Qiang Qiu[4], Yulin Chen[1,7,8], Lu Deng[1*], Zhipeng Li[2*], Xiaolong Wang[1,7,8*] and Ke Zhang[1*]

[†]Yu Lei, Yining Zheng, and Yiting Yan contributed equally to this work.

*Correspondence: denglu128128@nwafu.edu.cn; zhipengli@jlau.edu.cn; xiaolongwang@nwafu.edu.cn; kezhang@nwafu.edu.cn

[1] International Joint Agriculture Research Center for Animal Bio-Breeding, Ministry of Agriculture and Rural Affairs/Key Laboratory of Animal Genetics, Breeding and Reproduction of Shaanxi Province, College of Animal Science and Technology, Northwest A&F University, Yangling 712100, China
[2] College of Animal Science and Technology, Jilin Agricultural University, Changchun 130118, China
Full list of author information is available at the end of the article

Abstract

Background: The rumen microbiome is critical for regulating milk synthesis in dairy livestock, yet the molecular mechanisms linking microbial functions to host lipid metabolism remain poorly understood. While host genetics and microbial composition have been studied, integrative analyses of the rumen-blood-mammary gland axis remain lacking.

Results: Here, we present the goat rumen microbial reference gene catalog and 5514 metagenome-assembled genomes (MAGs) from 160 multi-breed rumen samples. Integrating this resource with lactation data from 177 Saanen dairy goats, we identify *Prevotella* spp. as keystone taxa driving concurrent increases in milk yield and fat percentage. Functional and metabolomic profiling reveals that *Prevotella bryantii* B14 synthesizes nicotinate, which is converted to nicotinamide in circulation. Using *in vitro* and *in vivo* models, we demonstrate that nicotinamide activates the mTORC1 pathway in mammary epithelial cells via GPR109A, which upregulates transcription factors *SREBP* and *PPAR-γ* and the downstream lipogenic genes *FASN*, *ACCa*, and *SCD1* to promote milk fat synthesis. In contrast, the relative deficiency of *P. bryantii* B14 and the associated reduction in nicotinamide levels in the rumen of poor lactating dairy goats may represent a significant contributor to impaired lactation performance. Additionally, the enhanced hydrogenotrophic methanogenesis activity may also adversely affect their lactation phenotype.

Conclusions: Our study establishes a causal link between rumen microbial metabolism and mammary lipid synthesis mediated by nicotinamide-mTORC1 signaling and identifies *Prevotella* abundance as a biomarker for precision breeding. These findings advance the understanding of microbiome-host crosstalk in lactation and provide actionable strategies for enhancing dairy productivity through microbiota-targeted interventions.

Background

The global demand for dairy products continues to rise, presenting the livestock industry with the dual challenges of improving production efficiency and achieving low-carbon outputs [1]. Among the determinants of dairy quality and economic value, milk fat content serves as a critical metric, directly influencing the nutritional profile and market returns of milk and its derivatives [2, 3]. Dairy goats represent an ideal model for elucidating the mechanisms of milk fat synthesis, due to their high milk fat bioavailability [4] and more pronounced responsiveness of milk fat changes induced by exogenous nutritional interventions through microbial mediation [5–7]. Additionally, goat milk, rich in short- and medium-chain fatty acids [8], is increasingly favored for producing infant formula. Despite progress, research into the regulatory effects of genetic [9, 10], nutritional [11], and environmental factors [12] on milk yield and milk fat percentage remains limited. Milk production and fat synthesis are governed by complex, synergistic interactions among multiple metabolic organs [13], yet the core functional nodes and specific metabolic regulatory mechanisms of the "rumen-blood-mammary gland" axis remain poorly understood [14]. Elucidating the multi-organ metabolic networks underlying high milk yield and high milk fat percentage phenotypes in dairy goats holds significant industrial relevance. Such insights could inform strategies to optimize dairy production systems, enhancing efficiency while supporting sustainable agricultural practices.

Current research on lactation performance in dairy livestock primarily focuses on individual lactation phenotypes, such as milk yield or milk fat synthesis [12, 15]. However, there is a lack of systematic and comprehensive understanding of the synergistic regulatory mechanisms between milk yield and milk fat percentage. This limitation hinders a holistic insight into the complexity of the mammary gland metabolic network and its multidimensional regulatory processes. Additionally, the rumen, as the central hub of the host-feed metabolism network, plays a pivotal role in these processes [16]. Rumen microbiota ferment dietary substrates to produce key metabolites such as volatile fatty acids (VFAs) [17], which serve as critical carbon sources and precursor compounds for milk and milk fat synthesis [18–20]. Despite this central role, the intricate complexity of the rumen metabolic network and the vast diversity of its microbial population pose substantial challenges in identifying core functional species [21]. Current research predominantly emphasizes macro-level correlations and predictive analyses of rumen microbial communities and their functions [4, 22, 23], with limited exploration of the direct causal relationships between specific microbes and milk fat synthesis. These gaps in knowledge hinder the development of robust theoretical frameworks and practical innovations for the precision regulation of dairy production performance.

To comprehensively investigate the key functional microbial species in the rumen associated with milk yield and milk fat synthesis, and to evaluate whether their metabolites regulate the metabolic system of dairy livestock via the "rumen-blood-mammary gland" axis through activation of specific mammary gland signaling pathways [14], this study first establishes the most comprehensive goat rumen microbial gene catalog (GRMGC) and a database of metagenome-assembled genomes (MAGs). Using a dual-factor control model that integrates high milk yield and high milk fat percentage, we systematically identify and analyze core functional nodes of the rumen microbiome within the host metabolic network. Our findings highlight the pivotal roles of specific

metabolic pathways and microbial functional modules in the "rumen-blood-mammary gland" axis [14], demonstrating their significant influence on the precursors and final synthesis of milk and milk fat. These processes are closely linked to the energy allocation mechanisms in dairy livestock. Through integrated in vivo and in vitro approaches, we confirm the metabolic contributions of a critical functional microbe, proposing a novel strategy for optimizing dairy livestock production performance via targeted microbial interventions. This study provides mechanistic insights into the molecular interplay between rumen metabolism and host milk fat synthesis, offering a theoretical foundation for improving production efficiency and mitigating the environmental impact of dairy farming. These findings advance the development of rumen-focused strategies for sustainable dairy production and provide actionable guidance for the dairy industry.

Results

Construction of the goat rumen microbial reference gene catalog

We constructed the GRMGC using metagenomic sequencing data from 160 rumen digesta samples spanning 8 goat breeds across 6 provinces in China. This dataset included 123 newly collected samples and 37 samples from published studies [24–27] (Fig. 1A and Additional file 1: Table S1). After stringent quality control to remove exogenous DNA contaminants, 3.03 Tb of high-quality sequencing reads were retained (Additional file 2: Fig. S1 and Additional file 3: Table S2). De novo assembly and open reading

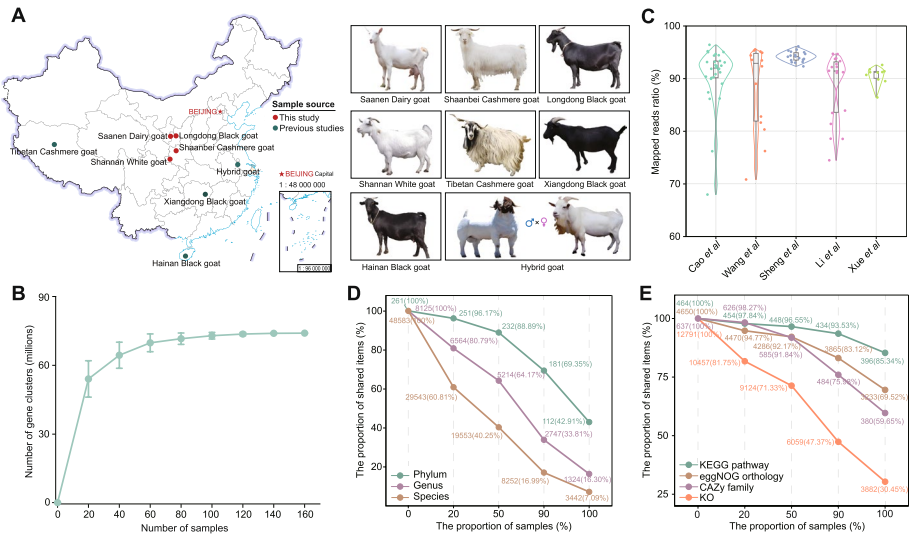

Fig. 1 Overview of the goat rumen microbial reference gene catalog (GRMGC). **A** This panel features a montage of the goat breeds described in this study. Red circles indicate newly collected rumen digesta samples, while green circles represent samples from previous studies obtained from the NCBI-SRA database. **B** Rarefaction analysis was performed using 100 random samplings without replacement to estimate the total number of NR predicted genes. Sample sizes ranged from 20 to 160, increasing by 20 samples per step. The mean values from 100 samplings for each sample size are plotted. **C** Alignment results of additional goat and sheep rumen metagenomic data with the GRMGC are shown. **D** The number (percentage) of shared bacterial taxa at the phylum (green), genus (pink), and species (yellow) levels across samples is depicted. The *y*-axis represents the percentage of shared items, while the *x*-axis shows the proportion of shared samples. Data for 20%, 50%, 90%, and 100% of the samples are highlighted. **E** The number and percentage of shared functional items in KEGG orthologs (orange), KEGG pathways (green), CAZy families (pink), and eggNOG orthology (yellow) are presented. Other legends are consistent with **D**

frame (ORF) prediction yielded 179.20 million contigs and 304.63 million ORFs, with 26.62% being complete (Additional file 4: Table S3). Clustering at 95% average nucleotide identity (ANI) resulted in 73,875,589 nonredundant (NR) genes, with an average length of 686 bp (Additional file 5: Table S4). Rarefaction analysis indicated that GRMGC captured the majority of microbial genes present in the goat rumen microbiome with saturation at approximately 80 samples (Fig. 1B). Comparative analyses revealed that minimal overlap of GRMGC with previously reported gene catalogs, including 14.2% with Xie et al. [26] and Li et al. [28] and only 4.19% with the rumen NR protein set by Stewart et al. [29] (Additional file 2: Fig. S2). Mapping of metagenomic reads from three independent goat [4, 30, 31] and two distinct sheep [32, 33] datasets demonstrated approximately 90% of quality-filtered reads were mapped (goats: 91.09%; sheep: 89.21%), highlighting unprecedented coverage by GRMGC (Fig. 1C). These results strongly support the necessity of constructing GRMGC, as there remains a vast reservoir of valuable microbial gene resources in the goat rumen microbiome awaiting discovery. Therefore, the construction of GRMGC will provide a crucial reference and baseline for further studies on the rumen microbiome of both goats and sheep.

Taxonomy and functional landscape of the goat rumen microbiome

To comprehensively characterize the taxonomic landscape of the goat rumen microbiome, we translated the NR predicted genes from the GRMGC into protein sequences and aligned them against the NCBI-NR database (version: October 2022). Of these, 85.13% successfully matched known proteins, while 14.87% remained unannotated as unknown proteins (Additional file 2: Fig. S3A). Among the NR predicted genes with assigned taxonomic information, 94.96% were classified as bacteria, 3.59% as archaea, and the remaining 1.05%, 0.39%, and 0.01% as viruses, fungi, and unclassified at the domain level, respectively (Additional file 2: Fig. S3B). At the phylum level, the NR predicted genes were predominantly annotated as Bacteroidota (47.87%), Firmicutes (37.64%), and Euryarchaeota (2.98%) (Additional file 2: Fig. S3C). Notably, a significant proportion of NR predicted genes (64.06%) lacked precise taxonomic assignment at the genus level. Among those successfully classified at the genus level, the majority were assigned to *Prevotella* (20.48%), *Methanobrevibacter* (2.81%), and *Ruminococcus* (2.03%) (Additional file 2: Fig. S3D). Furthermore, 181 phyla (representing 69.35% of all annotated phyla), 2747 genera (33.81%), and 8252 species (16.99%) were detected in over 90% of samples, thereby constituting core rumen microbiota in goats (Fig. 1D). The cumulative abundance of these core species accounted for more than 99.68% of the goat rumen microbiome composition. The dominant species with the highest relative abundance (TPM) included *Prevotella* sp., Bacteroidales bacterium, Clostridia bacterium, Oscillospiraceae bacterium, and Lachnospiraceae bacterium (Additional file 2: Fig. S3E).

Functional annotation of the NR predicted genes within the GRMGC was performed using the KEGG, CAZy, and eggNOG databases. Only 49.44%, 32.12%, and 3.88% of the genes were annotated as clusters of orthologous groups of proteins (COGs), KEGG orthologous groups (KOs), and carbohydrate-active enzymes (CAZymes), respectively. This indicates that the GRMGC contains a substantial proportion of genes with unidentified functions, representing a highly complex functional repertoire (Additional file 6: Table S5). The predominant functional capacities of the rumen microbiome in goats,

based on the GRMGC, are listed in Additional file 7: Table S6. Importantly, core KOs (47.37%), KEGG pathways (95.53%), CAZy families (75.98%), and eggNOG orthologous groups (83.12%) present in over 90% of the samples were significantly more prevalent than the proportion of core species (16.99%) (Fig. 1D, E). This indicates that the extensive presence of microbial species within the goat rumen microbiome exhibits functional redundancy, which may enhance the functional stability of the rumen microbiome and contribute to its resilience against external perturbations affecting rumen metabolic functions [34].

Phenotypic characteristics and taxonomic differences in HH and LL dairy goats

Building upon the successfully established GRMGC, we conducted an in-depth analysis to elucidate the biomarker microbial taxa within the rumen of high milk yield and high milk fat percentage (HH) goats and their regulatory roles in milk yield and milk fat synthesis. A cohort of 177 mid-lactation Saanen dairy goats, maintained under identical environmental conditions, was subjected to longitudinal monitoring (Additional file 8: Table S7). Ultimately, 10 HH and 10 low milk yield and low milk fat percentage (LL) dairy goats were selected for further analysis (see "Methods"; Fig. 2A and Additional file 8: Table S7). Comparative analyses of lactation phenotypes revealed that milk yield, milk fat percentage, milk fat yield (calculated as milk yield [kg/day] × milk fat [%]; MFY), and total solids were significantly elevated in the HH group compared to the LL group ($P < 0.05$, Fig. 2B, C, D, E), whereas milk protein percentage, milk lactose percentage, milk urea nitrogen concentration, and somatic cell count (SCC) did not differ significantly between the groups ($P > 0.05$, Additional file 2: Fig. S4A, B, C, D). Notably, concentrations of glucose, a biomarker for milk production, and β-hydroxybutyrate (BHBA), a key precursor for milk fat synthesis, were significantly increased in the HH group ($P < 0.05$, Additional file 9: Table S8), suggesting alterations in rumen carbon metabolism between HH and LL groups. Further analysis of rumen fermentation parameters indicated that as anticipated, the HH group exhibited significantly higher concentrations of total VFAs, acetate, propionate, butyrate, and valerate, alongside a reduced acetate/propionate ratio (A/P ratio) and lower pH levels ($P < 0.05$; Fig. 2F, G, H, I, J and Additional file 2: Fig. S4E, F). Conversely, concentrations of isobutyrate, isovalerate, and NH_3-N did not differ significantly between the two groups ($P > 0.05$; Additional file 2: Fig. S4G, H, I). These results suggest significant disparities in rumen fermentation profiles between HH and LL dairy goats.

We then identified the biomarker microbiota affecting lactation performance and rumen fermentation parameters in HH dairy goats based on the GRMGC. The HH group exhibited reduced microbial diversity in the rumen ($P < 0.05$; Additional file 2: Fig. S5) and significant segregation in microbial composition compared to the LL group (Bray–Curtis; PERMANOVA: $R^2 = 0.232$, $P = 0.004$; Fig. 2K). This differentiation was characterized by a significantly higher relative abundance of bacteria and a significantly lower relative abundance of archaea in the HH group ($P < 0.05$; Fig. 2L), along with variations observed at the phylum level (Additional file 2: Fig. S6). Notably, the relative abundances of *Prevotella* and *Bacteroides* were significantly elevated in the HH group ($P < 0.05$; Fig. 2M), whereas those of *Candidatus Methanomethylophilus*, *Methanosarcina*, and *Pyrococcus* were significantly reduced ($P < 0.05$; Fig. 2M). The differential

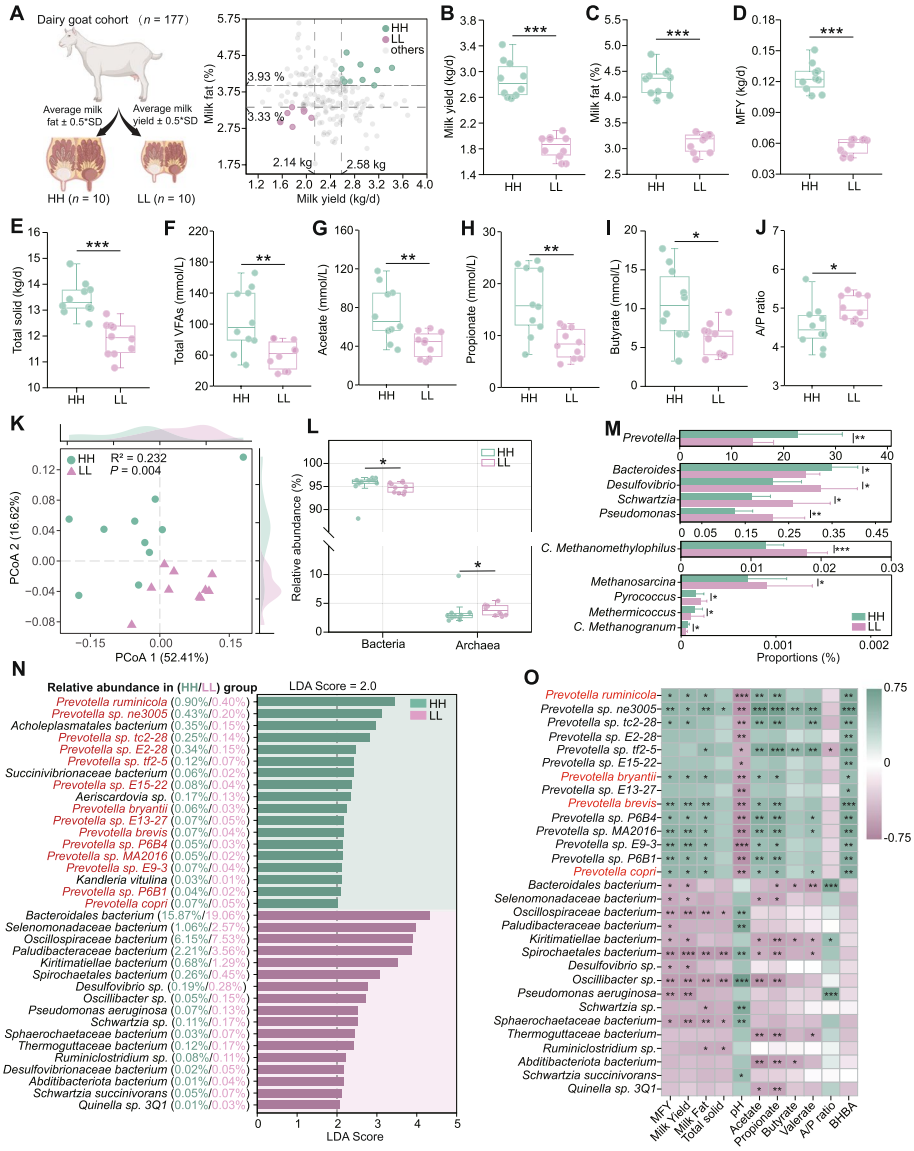

Fig. 2 Differences in lactation phenotypes, rumen fermentation parameters, and microbial composition between HH and LL dairy goats. **A** HH and LL dairy goats ($n = 10$/group) were selected from a cohort of 177 based on average milk yield and milk fat percentage (± 0.5 SD). Analysis of differences in lactation phenotypes, including milk yield (**B**), milk fat percentage (**C**), milk fat yield (MFY) (**D**), and total solids in milk (**E**) between HH and LL goats ($n = 10$/group). Statistical significance was determined using Student's *t-test*. ***$P < 0.001$. Differences in rumen fermentation parameters, including total VFAs (**F**), acetate (**G**), propionate (**H**), butyrate (**I**), and the acetate/propionate ratio (A/P) (**J**), were analyzed between HH and LL goats ($n = 10$/group). Statistical significance was determined using Student's *t-test*. *$P < 0.05$ and **$P < 0.01$. **K** Visualization of rumen microbiota profiles in HH and LL goats based on PCoA. Evaluation of Bray–Curtis dissimilarity using PERMANOVA ($n = 10$/group). **L** The Wilcoxon rank-sum test was used to identify significant differences in the relative abundance of bacterial and archaeal domains (**L**) and genera (**M**) between HH and LL dairy goats. Multiple testing correction using the Benjamini–Hochberg procedure ($n = 10$/group). *$P < 0.05$, **$P < 0.01$, and ***$P < 0.001$. **N** LEfSe analysis identified differential bacterial species between HH and LL groups, with linear discriminant analysis (LDA) scores indicating significant enrichment for taxa ($P < 0.05$, $|LDA| > 2$), treating all samples as independent ($n = 10$/group). **O** Spearman correlation analysis ($P < 0.05$, $|R| > 0.5$) examining the relationship between differentially enriched bacterial species and key phenotypes in HH and LL dairy goats ($n = 10$/group). *$P < 0.05$, **$P < 0.01$, and ***$P < 0.001$. Data involving error bars are presented as mean ± SEM. Abbreviation: C., Candidate

abundance of *Prevotella* between the two groups was further validated using absolute quantification ($P < 0.05$; Additional file 2: Fig. S7). Given the extensive diversity within the genus *Prevotella*, we further delineated differences at the species level, identifying *Prevotella ruminicola*, *Prevotella bryantii*, *Prevotella brevis*, *Prevotella copri*, and 10 unclassified *Prevotella* spp. as biomarker microbes in the HH group ($LDA > 2$, $P < 0.05$; Fig. 2N). Conversely, *Methanobrevibacter woesei* was identified as the biomarker archaea ($LDA > 2$, $P < 0.05$; Additional file 2: Fig. S8). To investigate the relationship between *Prevotella* spp. and lactation phenotypes, we conducted the Spearman correlation analysis and found the significantly positive correlations between *P. ruminicola*, *P. bryantii*, *P. brevis*, *P. copri* and milk yield, milk fat percentage, and MFY ($|R| > 0.5$, $P < 0.05$; Fig. 2O). These results suggest that *Prevotella* may serve as a key member of the rumen microbiota, potentially playing a pivotal role in enhancing milk yield and milk fat synthesis.

Differential microbial functional and metabolic profiles in HH and LL dairy goats

To preliminarily elucidate the differential metabolic cascades of the rumen microbiome in HH and LL dairy goats, functional annotation of the acquired microbial gene data was performed using the KEGG database. PCoA analysis based on KOs and KEGG module revealed that the HH and LL groups possessed significantly distinct functional metabolic profiles (Bray–Curtis; PERMANOVA KO: $P = 0.036$, $R^2 = 0.149$; PERMANOVA module: $P = 0.041$, $R^2 = 0.124$; Additional file 2: Fig. S9A, B). LEfSe analysis identified significant level 3 pathways enriched in the HH group, primarily involving alanine, aspartate, and glutamate metabolism (ko00250), propionate metabolism (ko00640), and nitrogen metabolism (ko00910) ($LDA > 2$, $P < 0.05$; Fig. 3A). At the KEGG module level, particular emphasis was placed on nicotinate and nicotinamide metabolism (ko00760), pantothenate and CoA biosynthesis (ko00770), and thiamine metabolism (ko00730). Downstream of these pathways, modules M00115 (converting aspartate to NAD^+), M00119 (converting valine/aspartate to pantothenate), M00120 (converting pantothenate to CoA), M00896 (converting AIR + [NAD^+] to TPP/TMP), and M00895 (converting AIR + [DXP/glycine] to TPP/TMP) were significantly enriched in the rumen of HH dairy goats, whereas modules M00563 (converting methylamine/dimethylamine/trimethylamine to methane) and M00345 (ribulose monophosphate pathway) under methane metabolism were significantly enriched in the rumen of LL dairy goats ($LDA > 2$, $P < 0.05$; Additional file 2: Fig. S10). Furthermore, non-targeted metabolomics revealed significant distinctions in the metabolite composition between the HH and LL dairy goats (Bray–Curtis; PERMANOVA: $P = 0.002$, $R^2 = 0.155$; Additional file 2: Fig. S9C). The differential metabolites were primarily involved in nicotinate and nicotinamide metabolism (ko00760), tyrosine metabolism (ko00350), and butanoate metabolism (ko00650) ($P < 0.05$, Rich factor > 0.5; Additional file 2: Fig. S11).

To thoroughly elucidate the differential metabolic functional characteristics of the rumen microbiota in HH and LL dairy goats, we integrated differential enzyme genes and metabolites and constructed schematic diagrams of rumen metabolism between the two groups (Fig. 3B and Additional file 2: Fig. S12). Specifically, we identified that the key enzyme genes *acdAB*, *pflD*, *pduL*, and *ackA*, which were involved in the conversion of acetyl-CoA and propanoyl-CoA to acetate and propionate, were

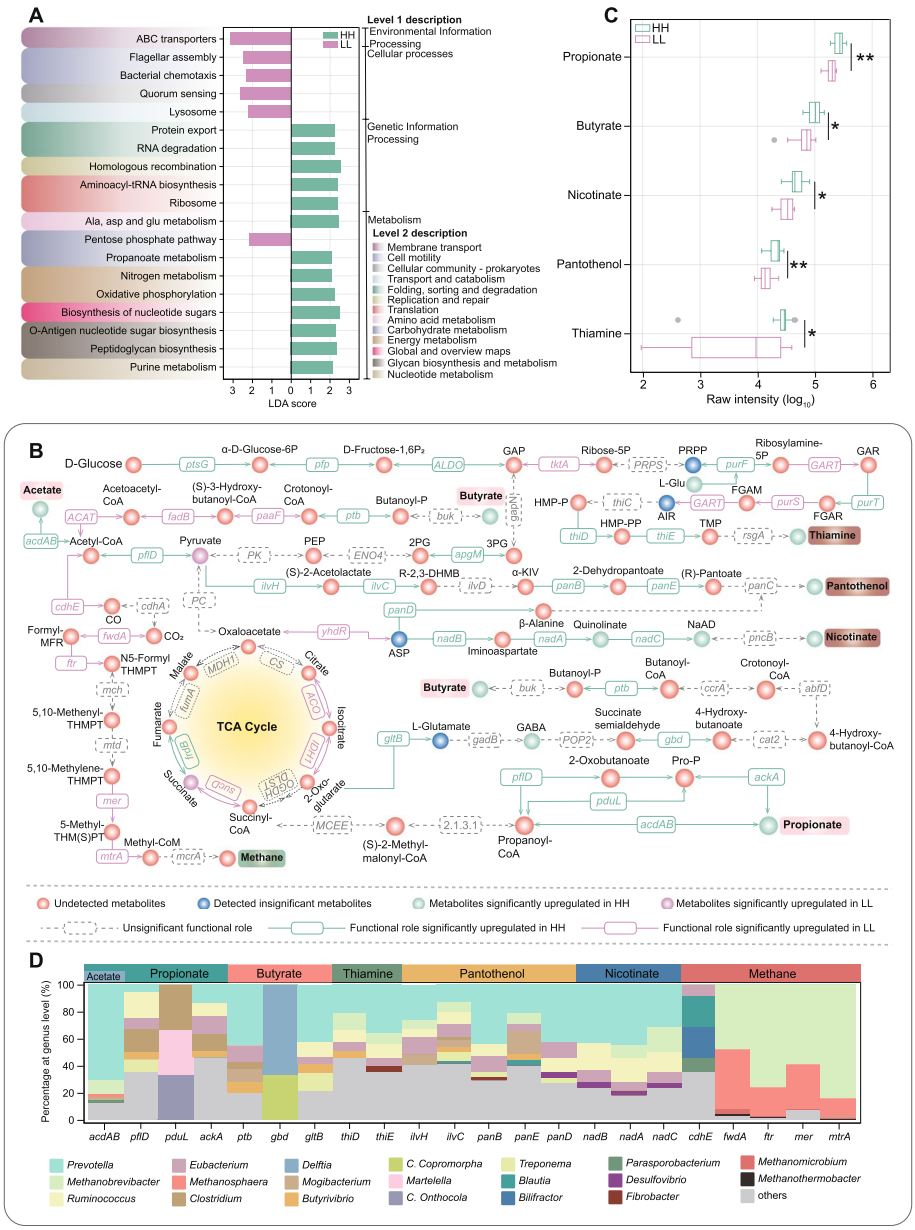

Fig. 3 Differential metabolic profiles of rumen microbiota in HH and LL dairy goats. **A** LEfSe analysis identified differentially enriched level 3 metabolic pathways in HH and LL dairy goats ($n = 10$/group). Significance was determined at $P < 0.05$ and $|LDA| > 2$. **B** Overview of rumen microbiota metabolic pathways. Metabolites are depicted as circles: undetected (orange), detected with no significant difference (blue), significantly increased in HH (green), and significantly increased in LL (pink). Enzyme genes are shown in gray dashed boxes (no significant difference), green solid boxes (upregulated in HH), and pink solid boxes (upregulated in LL). VFAs and B vitamins are highlighted with pink and brown backgrounds, respectively. Differences were tested using the Wilcoxon rank-sum test and Student's *t-test*. **C** Key metabolites with significant differences, including propionate, butyrate, nicotinate, pantothenol, and thiamine ($n = 10$/group). Statistical significance was determined using Student's *t-test*. $^{*}P < 0.05$ and $^{**}P < 0.01$. **D** Genus-level phylogenetic distribution of VFAs (acetate, propionate, butyrate), B vitamins (nicotinate, thiamine, pantothenol), and methane metabolism-related enzyme genes. Data involving error bars are presented as mean ± SEM. Abbreviations: Ala, alanine; asp, aspartate; glu, glutamate; GAP, glyceraldehyde 3P; 3PG, glycerate-3P; 2PG, glycerate-2P; PEP, phosphoenolpyruvate; Pro-P, propanoyl phosphate; GABA, 4-aminobutanoate; L-Glu, L-glutamine; ASP, L-aspartate; R-2,3-DHMB, (R)—2,3-dihydroxy-3-methylbutanoate; α-KIV, alpha-ketoisovalerate; NaAD, nicotinate D-ribonucleotide; C., candidate

significantly upregulated in the HH group, resulting in higher concentrations of acetate and propionate in the rumen of HH dairy goats ($P < 0.05$; Figs. 2G, 3B, C and Additional file 2: Fig. S12). Additionally, the primary pathway for butyrate biosynthesis (converting acetyl-CoA to butyrate) in the HH group involved the key enzyme gene *ptb*, and the alternative butyrate synthesis pathway (converting L-glutamate to butyrate) involved the key enzyme genes *gltB* and *gbd*, which were also expressed at higher levels in the HH group. This further led to a significant increase in butyrate concentration in the rumen of HH dairy goats ($P < 0.05$; Fig. 3B, C and Additional file 2: Fig. S12). Importantly, we observed elevated concentrations of thiamine, pantothenol, and nicotinate in the rumens of HH dairy goats ($P < 0.05$; Fig. 3C). Correspondingly, the relative abundances of the key enzyme genes involved in thiamine biosynthesis (*thiD* and *thiE*), pantothenol biosynthesis (*ilvH*, *ilvC*, *panB*, *panE*, and *panD*), and nicotinate biosynthesis (*nadB*, *nadA*, and *nadC*) increased in the HH dairy goats ($P < 0.05$; Fig. 3B and Additional file 2: Fig. S12). In contrast, compared to the HH dairy goats, the relative abundances of key enzyme genes involved in methane metabolism, including *cdhE*, *fwdA*, *ftr*, *mer*, and *mtrA*, were significantly higher in the LL group ($P < 0.05$; Fig. 3B and Additional file 2: Fig. S12A). To elucidate the source of these key enzyme genes, we examined their taxonomic distribution and found that the enzyme genes encoding the synthesis of three VFAs and three B vitamins were primarily annotated to *Prevotella*, while *Methanobrevibacter* was the main contributor to methane metabolism in the goat rumen (Fig. 3D). Thus, *Prevotella* may be a critical biomarker responsible for the elevated concentrations of three VFAs and three B vitamins in the rumen of HH dairy goats. Given that propionate, acetate, and butyrate are widely recognized as important metabolites influencing milk yield and milk fat percentage in dairy livestock [18–20], our subsequent studies focused primarily on a detailed analysis of the underlying causes of the suboptimal lactation phenotype in LL dairy goats and explored the contribution of *Prevotella* to the biosynthesis of nicotinate, thiamine, and pantothenol in the rumen.

Active hydrogen and methane metabolism in the rumen contribute to decreased lactation performance in LL dairy goats

Hydrogen, a natural byproduct of anaerobic fermentation in the rumen, is utilized by methanogenic archaea to produce methane, which is a key factor contributing to reduced energy efficiency and influencing lactation phenotypes in dairy livestock [35]. To comprehensively investigate the underlying causes of suboptimal lactation performance in LL dairy goats, we reconstructed 5514 MAGs meeting medium- or high-quality standards from deep metagenomic sequencing data of 160 rumen digesta samples using genomic binning techniques (Additional file 10: Table S9 and Additional file 11: Table S10). These MAGs were subsequently annotated using the hydDB database (Additional file 12: Table S11). Detailed information on the MAGs and hydrogenase profiles of the goat rumen microbiome can be found in the Additional file 2: Supplementary Results. Subsequently, using the Wilcoxon rank-sum test, we identified MAGs that were significantly upregulated in the HH and LL groups, respectively ($P < 0.05$; Additional file 13: Table S12). Upon comparing the H_2-producing fermentative hydrogenase (groups A1, A2, B FeFe-hydrogenases)

and H_2-producing electron bifurcating hydrogenase (group A3 FeFe-hydrogenases) predicted protein counts encoded by these significantly different MAGs [36], we found that the LL group had 1.63-fold more H_2-producing fermentative hydrogenase encoded by upregulated MAGs compared to the HH (951 *vs.* 585). Additionally, the LL possessed 2.53-fold more H_2-producing bifurcating hydrogenases than HH dairy goats (229 *vs.* 118) ($P < 0.05$; Fig. 4A). These results suggest that the rumen microbiome in the LL dairy goats possesses a more potent capacity for H_2 production. Furthermore, methanogenic hydrogenases (group 3a, 3c, 4 h, and 4i NiFe-hydrogenases, and Fe-hydrogenase) encoded by hydrogenotrophic methanogenic archaea facilitate the utilization of H_2 through the Wolfe cycle to promote methane synthesis [36]. Notably, five MAGs with significantly higher expression in the LL group exhibited elevated levels of these hydrogenases, with four identified as *Methanobacteria*. Conversely, MAGs with significant upregulation in the HH group seldom encoded these hydrogenases ($P < 0.05$; Fig. 4A). Further analysis of the ability of differentially upregulated MAGs to encode key enzyme genes involved in methane metabolism revealed that MAGs upregulated in the LL group could encode multiple key enzymatic steps in methane metabolism, whereas MAGs upregulated in the HH group largely lacked

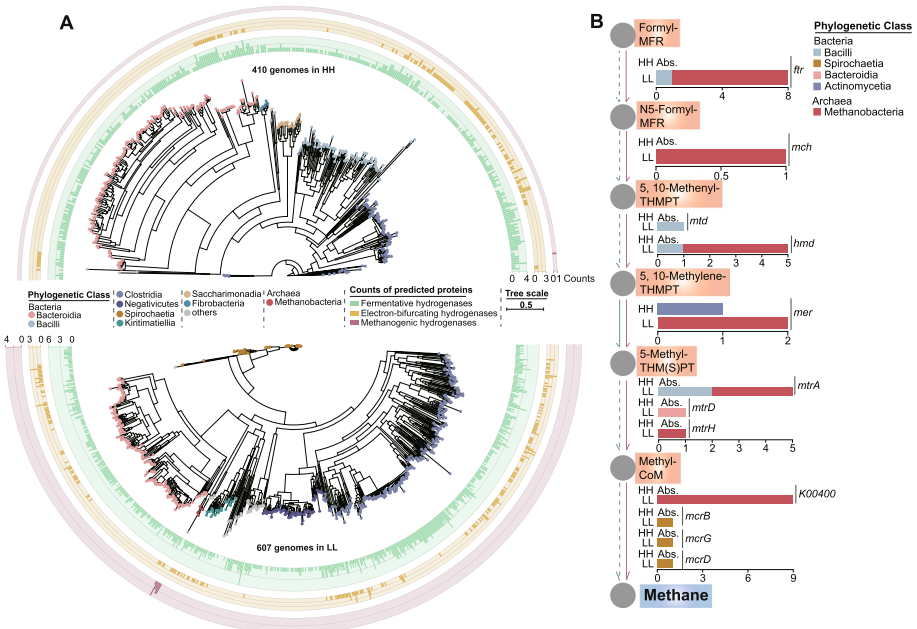

Fig. 4 Phylogenetic tree of H_2-producing hydrogenases and methane metabolism overview constructed from differential MAGs in HH and LL dairy goats. **A** Phylogenetic tree of H_2-producing hydrogenases constructed from MAGs differentially enriched in HH and LL groups. The upper semicircle represents MAGs significantly enriched in HH, while the lower semicircle represents those in LL. Differences were tested using the Wilcoxon rank-sum test, with significance at $P < 0.05$. Leaf nodes are colored according to class-level taxonomy. The inner and middle bar charts display predicted protein counts for H_2-producing fermentative hydrogenases (groups A1, A2, B FeFe-hydrogenases) and H_2-producing electron-bifurcating hydrogenases (group A3 FeFe-hydrogenases), respectively. The outer bar chart shows predicted protein counts for methanogenic hydrogenases. **B** Overview of methane metabolism constructed from MAGs with significant relative abundance (TPM) differences between HH and LL groups, tested using the Wilcoxon rank-sum test with a threshold of $P < 0.05$. Bar colors are based on class-level taxonomy of MAGs. Intermediate metabolites are highlighted with a yellow background, while the end product, methane, is highlighted with a blue background

the capability to encode these critical enzyme genes ($P < 0.05$; Fig. 4B). These findings robustly confirm that the rumen microbiome of the LL group enhances H_2 production and possesses a more formidable capacity to utilize H_2 for methane synthesis. This inefficient energy allocation pattern may ultimately contribute to the suboptimal lactation phenotype observed in the LL dairy goats.

Prevotella is the potent independent synthesizer of thiamine, pantothenol, and nicotinate in the rumen

To further validate the role of *Prevotella* in the biosynthesis of nicotinate, thiamine, and pantothenol within the rumen of dairy goats, ORFs from 5514 MAGs were translated into protein sequences and annotated with the KEGG database. We first characterized the unique biosynthetic pathways for nicotinate, thiamine, and pantothenol encoded by the goat rumen microbiome. Our analysis revealed that the rumen microbiome of dairy goats possesses a complete nicotinate biosynthetic capability. A substantial number of microbial-encoded enzyme genes support the biosynthesis pathways of nicotinate and nicotinamide (NAM) using L-aspartate as a precursor, and further biosynthesis of the

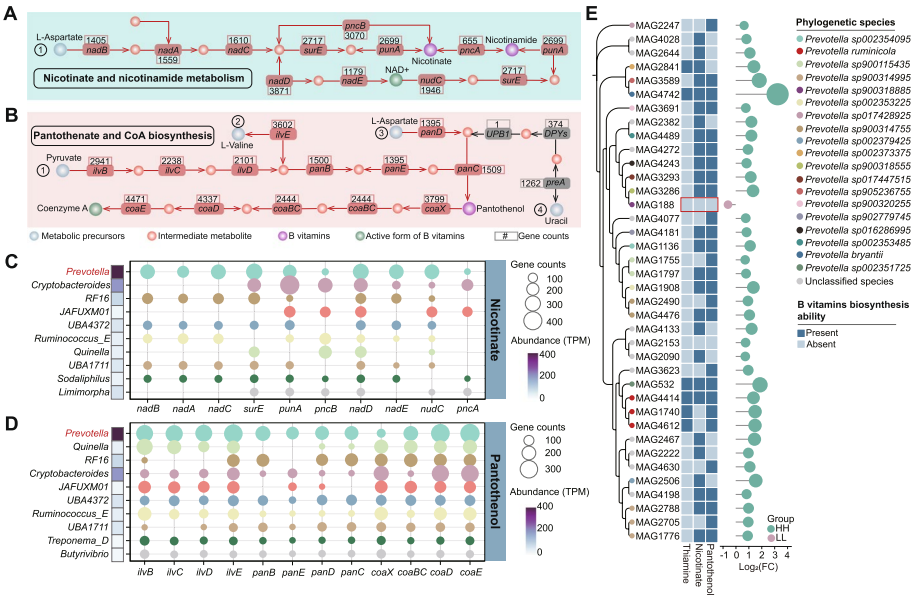

Fig. 5 *Prevotella* as a core genus in nicotinate and pantothenol biosynthesis within the goat rumen. Nicotinate (**A**) and pantothenol (**B**) biosynthesis pathways encoded by the goat rumen microbiome are illustrated. Cyan and orange circles represent metabolic precursors and intermediates, respectively, while pink and green circles denote target B vitamins and their functional coenzymes. Enzyme genes required for each pathway reaction are marked in orange boxes, with corresponding gene counts shown in overlapping hollow boxes. The bubble plots depict enzyme gene counts involved in nicotinate (**C**) and pantothenol (**D**) biosynthesis pathways across MAGs from different genera. Bubble size indicates enzyme gene counts, and color represents different genera. Only the top 10 genera with the most enzyme genes for nicotinate or pantothenol biosynthesis are shown. The left heatmap displays genus relative abundance (TPM) based on integrated MAGs. **E** Analysis of premium *Prevotella* MAGs with significant differences in thiamine, nicotinate, and pantothenol synthesis capabilities between HH and LL dairy goats. Premium *Prevotella* MAGs are defined as having completeness > 80% and contamination < 10%. Statistical significance was tested using the Wilcoxon rank-sum test ($P < 0.05$). The phylogenetic tree on the left illustrates the relationships of *Prevotella* MAGs, with leaf nodes colored by species. The middle binary heatmap indicates whether MAGs possess all enzyme genes for synthesizing the corresponding B vitamins. The lollipop chart shows *Prevotella* MAGs with significantly increased relative abundance (TPM) in HH or LL, based on $\log_2$(FC)

functional coenzyme form NAD^+ is facilitated by the enzyme genes *nadD* and *nadE* (Fig. 5A). Additionally, seven thiamine biosynthetic precursors are primarily characterized in the KEGG database. However, due to the absence of the key enzyme genes *tenI* and *thi4*, the thiamine synthesis pathway mediated by the rumen microbiome of dairy goats utilizes aminoimidazole ribotide as the precursor. Intermediate metabolites are converted into thiamine through the catalysis of *thiC*, *thiD*, *thiE*, *phoA*, and *rsgA* and subsequently transformed into the essential coenzyme thiamine diphosphate via *thiN* (Additional file 2: Fig. S13A). Upon examining the KOs associated with pantothenol biosynthesis in the goat rumen, we identified L-valine, pyruvate, and L-aspartate as the primary precursor substrates for pantothenol biosynthesis. In contrast, Uracil may exhibit reduced conversion efficiency due to the scarcity of *UPB1*. These three substrates undergo sequential catalysis by multiple enzyme genes and are ultimately synthesized into pantothenol under the influence of the central enzyme gene *panC*. Pantothenol is further converted into its active coenzyme by *coaX*, *coaBC*, *coaD*, and *coaE* (Fig. 5B). These results revealed the unique biosynthetic pathways for nicotinate, thiamine, and pantothenol encoded by the goat rumen microbiome, which serve as a critical foundation for subsequent analyses of the contribution of *Prevotella* to the synthesis of these three vitamins.

We then assessed the capability of MAGs from various genera in the rumen microbiome to synthesize these three B vitamins. Regarding nicotinate biosynthesis, among the top 10 genera in the goat rumen encoding the highest nicotinate synthase enzyme genes, *Prevotella* was the sole genus encompassing a complete nicotinate biosynthetic pathway and encoding the majority of key enzyme genes involved in nicotinate biosynthesis, thereby making it the primary nicotinate synthesizer within the rumen microbiome of dairy goats (Fig. 5C). Furthermore, MAGs annotated as *Cryptobacteroides* encoded the highest thiamine biosynthesis-related enzyme gene counts, followed by MAGs annotated as *Quinella*. However, *Cryptobacteroides* lacks *thiC* in the critical steps of thiamine biosynthesis, which may necessitate reliance on enzyme genes encoded by other microbes for thiamine biosynthesis. Although MAGs annotated as *Prevotella* encoded the third highest thiamine biosynthesis-related enzyme gene counts across all genera, they did not exhibit any absences of key enzyme genes (Additional file 2: Fig. S13B). Similarly, MAGs identified as *Prevotella* possessed complete pathways for pantothenol and CoA biosynthesis and contained the highest enzyme gene counts (Fig. 5D).

We then screened 392 MAGs annotated as *Prevotella* and clustered these MAGs together with all *Prevotella* genomes from the NCBI-RefSeq and NCBI-GenBank databases into species-level genome bins (SGBs) using a 95% ANI. The *Prevotella* SGBs obtained in this study expanded the phylogenetic relationships of *Prevotella* species by 15.91% (Additional file 2: Fig. S14). To identify the functional differences in the synthesis of thiamine, nicotinate, and pantothenol among highly abundant *Prevotella* MAGs in the rumen of HH and LL dairy goats, we selected premium *Prevotella* MAGs (defined as completeness > 80%, contamination < 10%) and utilized the MetaWrap "quant_bins" module to calculate the relative abundance (TPM) of these MAGs in HH and LL groups [37, 38]. We found 38 MAGs with significant differences between the two groups (Wilcoxon rank-sum test),

of which 37 MAGs had significantly higher relative abundance in the HH group ($P < 0.05$; Additional file 14: Table S13). Among the 37 MAGs, only one unclassified *Prevotella* MAG lacked the ability to synthesize all three B vitamins. In addition, 40.54% (15/37) of these MAGs could independently synthesize one B vitamin, 48.65% (18/37) could synthesize two B vitamins, and three MAGs encoded all enzyme genes required for the synthesis of thiamine, nicotinate, and pantothenol. Notably, MAG4742 (*P. bryantii*) and MAG4414 (*P. ruminicola*) were capable of independently synthesizing thiamine, nicotinate, and pantothenol. Additionally, only MAG188, annotated as *Prevotella* sp900318885, was significantly upregulated in the LL group; however, this MAG did not independently encode the synthesis pathways for the aforementioned three B vitamins (Fig. 5E). These findings substantiate that *Prevotella* is an indispensable functional genus for the biosynthesis of nicotinate, thiamine, and pantothenol in the rumen of dairy goats and suggest the need for further investigation into the impact of these endogenous B vitamins on the lactation biology of dairy goats.

P. bryantii B14 synthesizes nicotinate to activate mTORC1 via a GPR109A-dependent manner in the mammary gland

To elucidate the regulatory role of *Prevotella* spp. in dairy goat lactation, we enriched and cultivated the rumen-derived *P. bryantii* B14 (PB14). Since *Prevotella* is not the predominant contributor to thiamine biosynthetic enzymes and pantothenol/pantothenate interconversion occurs rapidly in the rumen, nicotinate was selected as the target metabolite for functional validation [39]. The whole-genome KEGG annotation of PB14 confirmed that it encodes a complete nicotinate biosynthesis pathway capable of converting L-aspartate to nicotinate (Fig. 6A). Growth kinetics identified early exponential (8 h), mid-exponential (11 h), and stationary (15 h) phases (Additional file 2: Fig. S15). We inoculated medium 159 (M159) with 1×10^8 CFU/mL PB14 (PB) or heat-inactivated PB14 (DPB). After 24 h, the PB group showed a significant reduction in L-aspartate and an increase in nicotinate compared to DPB ($P < 0.05$; Fig. 6B, C), confirming PB14's ability to synthesize nicotinate from L-aspartate. To assess the impact of PB14 on methane production, we introduced PB14 into an artificial rumen fermentation system (Fig. 6D). After setting up the system, we added 1×10^8 CFU/mL of PB14 (PB) or filtered, sterilized culture supernatant (SN). Inoculation with PB14 significantly reduced gas and methane production and markedly decreased the copy numbers of methanogenic archaea compared to the SN group ($P < 0.05$; Fig. 6E, F, G).

Subsequently, to validate the effects of PB14 on rumen fermentation and lactation performance in vivo, we administered a daily dose of 1×10^{11} CFU/L of PB14 to late-lactation dairy goats (Fig. 6H). Maintaining consistent average feed intake (Additional file 2: Fig. S16), PB14 administration mitigated the decline in average milk yield during the late lactation period (average decline 0.115 kg *vs.* average decline 0.036 kg) (Fig. 6I) and significantly enhanced milk fat percentage ($P < 0.05$; Fig. 6J). Further absolute quantification confirmed a significant increase

in PB14 copy numbers in the rumen of the PB group ($P < 0.01$; Additional file 2: Fig. S17A). Additionally, concentrations of total VFAs, acetate, propionate, and valerate were significantly elevated in the PB group ($P < 0.05$; Additional file 2: Fig. S18). Consistent with in vitro findings, PB14 colonization in the rumen of dairy goats facilitated nicotinate synthesis ($P < 0.05$; Additional file 2: Fig. S19) and significantly reduced the copy numbers of methanogenic archaea ($P < 0.05$; Additional file 2: Fig. S17B). These results suggest that PB14 is a stable colonizer and efficient producer of nicotinate in the rumen, contributing to improved lactation performance in dairy goats.

To elucidate the molecular mechanisms by which PB14-mediated increases in nicotinate levels regulate milk fat synthesis in the mammary gland, we quantified the serum concentration of NAM, the circulating form of nicotinate, in HH and LL dairy goats [40]. The results demonstrated that the concentration of NAM in the HH group was significantly higher than that in the LL group ($P < 0.01$; Fig. 6K). Moreover, the selected NAM concentrations did not affect bovine mammary epithelial cells (MAC-T) proliferation (Additional file 2: Fig. S20), while 0.5-mM NAM treatment significantly increased the expression of lipogenic genes *ACCα*, *SREBP*, *FASN*, *PPAR-γ*, and *SCD1* ($P < 0.05$; Fig. 6L). To further explore the critical signaling pathways through which NAM influences milk

(See figure on next page.)

Fig. 6 *P. bryantii* B14 synthesizes nicotinate to activate mTORC1 and enhance milk fat synthesis. **A** Morphology and whole-genome map of *P. bryantii* B14. The left panel shows the morphological features of *P. bryantii* B14 at 6000 × and 20,000 × magnification. The right genome circle map displays the size of the *P. bryantii* B14 genome in Mb in the innermost ring. The second ring (gray) shows the GC percentage of the *P. bryantii* B14 genome. The third ring uses red and blue to indicate positive and negative GC skew, respectively. The outermost ring highlights the coding sequences in green. Quantification of L-aspartate (**B**) and nicotinate (**C**) in the culture medium 24 h after inoculation of the culture tubes with *P. bryantii* B14 (PB) and heat-killed *P. bryantii* B14 (DPB), respectively ($n = 3$/group). Statistical significance was determined using Student's *t-test*. $^{*}P < 0.05$. **D** Schematic of the in vitro simulated rumen system. Briefly, anaerobic gas collection bags are used to collect gases produced by anaerobic fermentation. The gas volume is measured using a syringe, and gas composition is determined by gas chromatography; anaerobic fermentation lasts for 24 h. Gas production (**E**), CH4 production (**F**), and methanogenic archaea copy numbers (**G**) after 24 h of anaerobic fermentation in bottles inoculated with *P. bryantii* B14 culture supernatant (sterilization using a 0.22-μm filter membrane; SN) or active *P. bryantii* B14 (PB) ($n = 3$/group). Statistical significance was determined using Student's *t-test*. $^{*}P < 0.05$ and $^{**}P < 0.01$. **H** Late-lactating dairy goats ($n = 5$/group) were grouped based on the presence (PB) or absence (CON) of *P. bryantii* B14 treatment. The entire experimental period spanned 17 days, comprising a 7-day adaptation phase followed by a 10-day treatment phase. **I** Changes in average milk yield of goats during the adaptation and treatment periods. Goats not treated with *P. bryantii* B14 (CON) showed a decrease in average milk yield of 0.115 kg from the adaptation to the treatment period, whereas *P. bryantii* B14 treatment (PB) reduced this decrease to 0.036 kg ($n = 5$/group). **J** Analysis of milk fat percentage in goats on the last day of the adaptation period (7 days) and on the fifth (12 days) and tenth (17 days) days of the treatment period ($n = 5$/group). Statistical significance was determined using Student's *t-test*. $^{*}P < 0.05$ and $^{**}P < 0.01$. **K** Analysis of nicotinamide (NAM) content in the serum of HH and LL dairy goats (HH: $n = 9$, LL: $n = 7$). Statistical significance was determined using Student's *t-test*. $^{**}P < 0.01$. **L** Effect of NAM treatment at varying concentrations on lipid synthesis expression in bovine mammary epithelial cells (MAC-T) ($n = 3$/group). Statistical significance was determined using one-way ANOVA, followed by LSD test. $^{*}P < 0.05$, $^{**}P < 0.01$, and $^{***}P < 0.001$. **M** Western blot analysis of p-T389-S6K and p-S6 expression levels in MAC-T following gradient NAM treatment. **N** Effect of NAM on the expression of lipid synthesis genes *ACCα*, *SREBP*, *FASN*, *PPAR-γ*, and *SCD1* in MAC-T following mTORC1 inhibition, assessed using qRT-PCR ($n = 3$/group). The significance of the differences was tested using Student's *t-test*. $^{*}P < 0.05$ and $^{**}P < 0.01$. **O** Western blot analysis showing the impact of gradient NAM concentrations on p-T389-S6K and p-S6 expression levels after siGPR109A. **P** Effect of NAM on the expression of lipid synthesis genes *ACCα*, *SREBP*, *FASN*, *PPAR-γ*, and *SCD1* following siGPR109A was assessed using qRT-PCR ($n = 3$/group). The significance of the differences was tested using Student's *t-test*. $^{*}P < 0.05$, $^{**}P < 0.01$, and $^{***}P < 0.001$

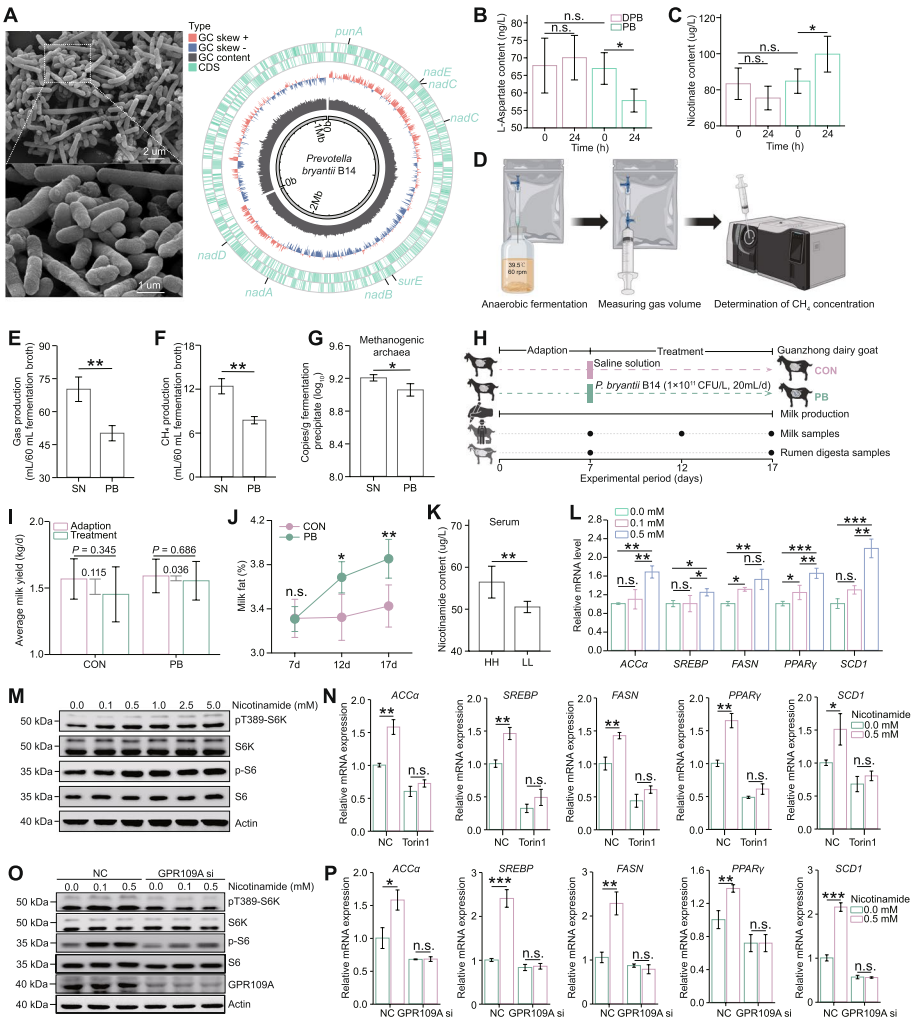

Fig. 6 (See legend on previous page.)

fat synthesis, we assessed the activation states of mechanistic target of rapamycin complex 1 (mTORC1), ERK, AMPK, and MAPK after treating MAC-T with gradient concentrations of NAM. We observed that NAM treatment at 0.5 mM significantly increased the protein expression levels of pT389-S6K and p-S6 in MAC-T, indicating the activation of mTORC1 (Fig. 6M and Additional file 2: Fig. S21). Inhibition of mTORC1 using Torin1 abrogated the regulatory effects of NAM on the downstream target genes *ACCα*, *SREBP*, *FASN*, *PPAR-γ*, and *SCD1* (Fig. 6N), thereby confirming that NAM enhances lipid synthesis in the mammary gland through an mTORC1-dependent pathway. Previous studies have identified the GPR109A as the receptor for nicotinate [41]. Therefore, we employed specific siRNA to knock down the expression of GPR109A in MAC-T ($P < 0.01$; Fig. 6O and Additional file 2: Fig. S22) and observed that NAM ceased to regulate the levels of pT389-S6K and p-S6 or the expression of the lipid synthesis genes *ACCα*, *SREBP*, *FASN*, *PPAR-γ*, and *SCD1* (Fig. 6P). To investigate the potential signaling connection between GPR109A and mTORC1 residing in distinct cellular compartments, we employed the selective PKA inhibitor H89. In the context of GPR109A knockdown, H89 partially restored NAM-induced mTORC1 activity, suggesting that PKA inhibition

is a key downstream regulatory event in NAM–GPR109A-mediated mTORC1 activation (Additional file 2: Fig. S23). In summary, our studies confirmed that NAM activates mTORC1 in a GPR109A-dependent manner and enhances milk fat synthesis by promoting the expression of downstream lipid synthesis-related genes.

Discussion

Enhancing milk yield and quality in dairy livestock is paramount for mitigating dairy product shortages and alleviating the environmental pressures associated with their growing populations [1]. A meticulous analysis of the microbial composition and functional attributes of the rumen in dairy livestock exhibiting varying lactation performances is invaluable for selective breeding and the formulation of precise nutritional strategies. In this study, we performed deep metagenomic sequencing on a cohort of 160 goats differing in breed, age, sex, habitat, and feeding regimes. This extensive analysis facilitated the creation of the most comprehensive goat rumen microbial reference gene catalog (GRMGC) and MAG database to date, substantially advancing our systematic understanding of the goat rumen microbial ecosystem [42]. Furthermore, our study systematically elucidated the critical role of the core rumen genus *Prevotella* in the biosynthesis of thiamine, nicotinate, and pantothenol. We also found that the relative deficiency of the PB14 and its associated reduction in NAM biosynthesis in LL individuals may represent a major contributor to impaired lactation performance. In addition, we observed an enhancement of hydrogenotrophic methanogenesis pathways in the rumen microbiome of LL individuals, which may be related to alterations in the rumen metabolic environment. However, the direct contribution of this shift to the decline in lactation performance remains to be further investigated. To establish a causal relationship between the rumen-blood-mammary gland axis and the augmentation of milk fat synthesis in dairy livestock, we employed multiple in vivo and in vitro models. These models revealed that the core rumen strain PB14 utilizes L-aspartate as a precursor to synthesize nicotinate. In the mammary gland, nicotinate, in its active form NAM, activates the mTORC1 signaling pathway in a GPR109A-dependent manner. This activation leads to the upregulation of the transcription factors *SREBP* and *PPAR-γ*, subsequently enhancing the expression of lipid synthesis-related genes *SCD1*, *FASN*, and *ACCα*, thereby promoting milk fat synthesis [43] (Fig. 7). In summary, this study underscores the significance of the rumen-blood-mammary gland axis as a framework for investigating lactation performance in ruminants and provides essential strains and theoretical foundations for the selective breeding of high-quality dairy livestock.

A distinguishing aspect of this study is the integration of diverse goat rumen samples from various regions, coupled with the construction of the GRMGC and goat rumen MAGs databases through deep metagenomic sequencing. These data resources revealed that the goat rumen microbiome remains largely unexplored, with 14.87% of NR predicted proteins remaining uncharacterized and over 50% of the phylogenetic relationships among microbial species yet to be elucidated. Furthermore, building upon prior rumen NR gene and protein catalogs [26, 28, 29], our study delivers the most comprehensive dataset to date. Although differences in assembly strategies may affect gene prediction, the sequence identity and coverage thresholds applied during redundancy filtering help to minimize these potential biases. Notably, the GRMGC generated in this

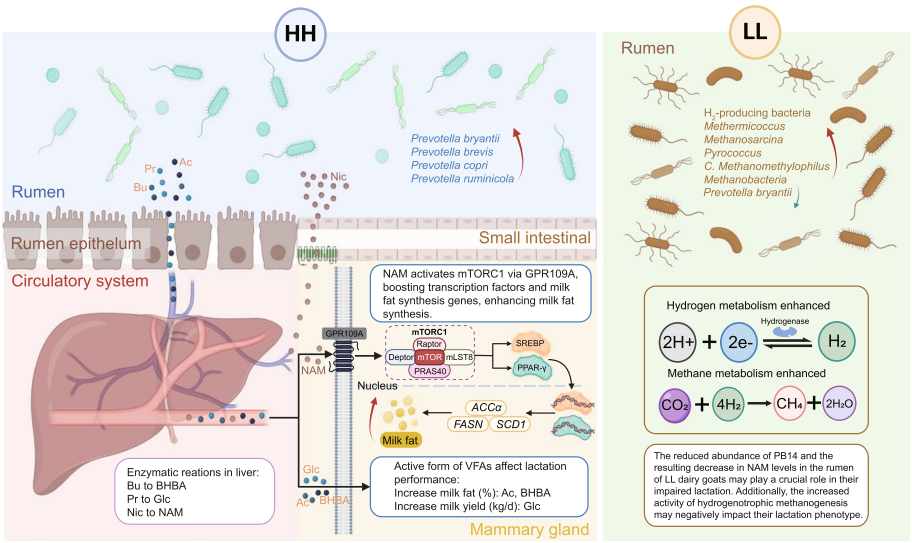

Fig. 7 Distinct rumen microbial metabolic functions in HH and LL dairy goats lead to contrasting lactation phenotypes. This scheme illustrates that the enrichment of *Prevotella* spp. in the rumen of HH dairy goats leads to increased levels of propionate, acetate, butyrate, and nicotinate. These metabolites are converted in the liver and enter mammary epithelial cells as glucose, acetate, BHBA, and NAM, respectively. Glucose serves as a precursor for lactose synthesis, influencing milk yield, while acetate and BHBA affect de novo milk fat synthesis pathways. Specifically, the active form of nicotinate, NAM, activates the mTORC1 signaling pathway via GPR109A, upregulating transcription factors *SREBP* and *PPAR-γ*, thereby promoting the expression of lipid synthesis-related genes *SCD1*, *FASN*, and *ACCα*, ultimately enhancing milk fat synthesis. Conversely, the relative scarcity of *P. bryantii* B14 and the consequent decrease in NAM levels in the rumen of LL dairy goats could be a key factor contributing to their impaired lactation. Moreover, the increased activity of hydrogenotrophic methanogenesis may further negatively impact their lactation phenotype. Abbreviations: Pr, propionate; Bu, butyrate; Ac, acetate; Nic, nicotinate; BHBA, *β*-hydroxybutyrate; Glc, glucose; NAM, nicotinamide; PB14, *Prevotella bryantii* B14

study, together with the gastrointestinal microbial gene catalog reported by Xie et al. [26], includes a broader range of host genetic backgrounds and encompasses a wider spectrum of dietary types and environmental niches. This broader representation results in a more complete and functionally relevant microbial gene resource. These findings underscore the importance of future studies aimed at systematically developing species-specific microbial gene catalogs for different gastrointestinal compartments in ruminants, under diverse host, dietary, and ecological conditions.

In parallel, we characterized the composition and functional features of the core rumen microbiota in HH dairy goats, revealing patterns partially consistent with previous studies [4, 22, 23]. However, to our knowledge, other associations have not yet been causally validated using in vivo and in vitro models. We identified a functional microbial community (FMC) centered around *Prevotella* spp. in the goat rumen. The FMC is highly enriched in HH dairy goats, and the representative strain PB14 has demonstrated significant biological roles in promoting nicotinate biosynthesis and inhibiting methane production. Importantly, FMC was also identified as a biomarker in the rumen of dairy cows with high milk yield and high milk protein percentage in previous studies, where it was considered to regulate milk protein percentage by modulating host amino acid metabolism [22]. Moreover, in a research cohort of 304 dairy cows, FMC was identified as a highly heritable microbiota and showed a

significant positive correlation with lactation phenotypes and the concentrations of VFAs in the rumen [23]. FMC is likely a core functional community that regulates the lactation performance of dairy livestock, prompting us to attempt to assemble FMC in vitro to better support research on the lactation performance of dairy livestock.

GPR109A, acting as the receptor for nicotinate, is highly expressed in the mammary gland [41]. Its activation induces the dissociation of the Gαi subunit [44], whereby the Gαi subunit inhibits the activity of adenylate cyclase, thereby reducing the production of cAMP and subsequently activating the mTORC1 signaling pathway [45, 46]. However, based on nicotinate kinetics in goats, NAM is likely the primary circulating form in the circulatory system of dairy goats [40], and the interaction between GPR109A and NAM remains unclear. Although we confirmed that GPR109A serves as a critical receptor mediating NAM-induced activation of mTORC1 by disrupting GPR109A expression, the specific regulatory mechanisms still require further elucidation. Additionally, to explain that the dosage of NAM treatment may exert markedly different effects on mTOR, higher concentrations of NAM (> 5 mM) can phosphorylate TSC2 (tuberin) in an AMPK-dependent manner or directly disrupt the interaction between mTORC1 and Raptor, thereby inhibiting mTORC1 [47, 48]. However, treatment with higher concentrations of NAM does not accurately reflect the changes in NAM concentration within the circulatory system (typically at the μM level [49–51]) and its impact on mTORC1. Therefore, we used a 0.5-mM NAM treatment for 4 h on MAC-T to mimic endogenous NAM effects, which activated the mTORC1 signaling pathway. Although a reasonable concentration of NAM was selected to replicate its endogenous effects on milk fat synthesis, the increase in NAM concentration mediated by the rumen microbiota may provide sustained and stable stimulation to the mammary gland. Therefore, further validation of these molecular findings in the mammary tissues of dairy livestock is crucial to ensure their applicability and accuracy.

Our study had several limitations. In the trial evaluating the effects of PB14 on lactational phenotypes in dairy goats, local temperature fluctuations may have interfered with feed intake in dairy goats [52]. Concurrently, constrained by biological characteristics of the caprine lactation cycle, this study employed a late-lactation model to assess the effects of PB14 on milk production performance. These factors may have compromised the objectivity in evaluating the lactogenic efficacy of PB14 [53]. Thus, future studies will employ a more stable mid-lactation model [22] to investigate the effects of PB14 on lactation phenotypes. Furthermore, we validated the NAM–GPR109A–mTORC1 signaling cascade solely in the MAC-T cell line, which may not fully capture the overall regulatory context of the mammary gland, including its structural organization and immune microenvironment. Therefore, further in-depth studies and validation of this mechanism are urgently needed in the dairy goat. Thirdly, although in vitro studies confirmed that the nicotinate-producing function of PB14 serves as a pivotal node connecting the rumen-blood-mammary gland axis, the functionality of PB14 may not fully represent the effects of the FMC. This is because the genotypic diversity introduced by complex microbial ecosystems can enhance metabolic adaptability and ecosystem functionality [54], thereby reflecting outcomes that are not observable within single-strain culturing systems. Consequently, we recommend the construction of anaerobic culturing systems

for FMC to thoroughly investigate interspecies interactions and regulatory mechanisms at the cellular level, thereby providing foundational data for FMC industrial applications.

Conclusions

Our study provides the most direct evidence to date supporting the regulation of milk fat synthesis by the rumen-blood-mammary gland metabolic axis in dairy livestock. Notably, we established a causal link between nicotinate synthesized by PB14, converted to its active form NAM, and the activation of mTORC1 in the mammary gland, thereby modulating milk fat synthesis. Crucially, we demonstrated that the regulatory effect of NAM on mammary gland mTORC1 at physiological concentrations is fundamentally distinct from that at pharmacological doses. Furthermore, we emphasize that the abundance of *Prevotella* spp. is as vital as host functions and represents an indispensable functional component within the rumen of dairy livestock. Consequently, the abundance of *Prevotella* spp. can be incorporated as a critical marker-assisted selection trait in breeding programs.

Methods

Additional methodological details, including the feeding regimen for dairy goats, preparation of the PB14 suspension, VFAs quantification, microbial DNA extraction, library construction and metagenomic sequencing, as well as the absolute quantification of microbial copy numbers, were comprehensively documented in the Additional file 2: Supplementary Methods.

Experimental setup, animal measurements, and sampling

A total of 177 healthy mid-lactation Saanen dairy goats (average parity: 2.20 ± 0.48, days in milk [DIM]: 121.50 ± 8.05; mean $\pm$ standard deviation [SD]) were selected from a commercial dairy goat farm. All animals were housed in the same well-ventilated barn and subjected to twice-daily milking sessions at 5:00 and 17:00, followed by feeding immediately after each milking. The dietary formulation for the dairy goats is detailed in Additional file 15: Table S14; the detailed feeding protocol is provided in the Additional file 2: Supplementary Methods. Milk yield data were collected daily during the first and fourth weeks of September 2022. The mean daily milk yield for each goat was calculated based on the average of the 2 weeks of daily measurements. On the final sampling day, milk was collected before each milking at a morning-to-evening volumetric ratio of 3:2. Milk components, including milk protein, milk fat, lactose, total solid, and SCC, were quantified using a milk composition analyzer (FOSS-4000, FOSS Electric A/S, Hillerød, Denmark) as outlined in Additional file 8: Table S7. Urea nitrogen levels in milk were measured using a urea nitrogen assay kit (ml016913, Mlbio, Shanghai, China). Previous studies indicated an inverse relationship between milk yield and milk fat percentage in dairy livestock [55]. Accordingly, goats were grouped based on their average milk yield and milk fat percentage, defined as mean $\pm 0.5 \times$ SD, resulting in the selection of 10 HH and 10 LL individuals (Fig. 2A and Additional file 8: Table S7). MFY was calculated as the product of average milk yield (kg/day) and milk fat (%). Using G*Power [56], the effect size for milk yield was calculated based on intergroup means and SDs,

followed by estimation of statistical power using a two-tailed independent-samples *t-test* at $\alpha = 0.05$. This analytical procedure was identically applied to milk fat percentage data. Calculations revealed that statistical power > 99% for both milk yield and milk fat percentage. Following classification, HH and LL goats were individually housed and fed, with feed intake recorded over a period of 3 days. The average daily feed intake for each goat was determined as the mean of the 3-day intake values (*HH*: 2.27 ± 0.29 kg/day; *LL*: 2.18 ± 0.25 kg/day; mean ± SD). Subsequently, rumen digesta samples from HH and LL goats were collected via oral gastric tubing before morning feeding. The samples were then used for VFA analysis and the quantification of *Prevotella* copy numbers [57] (see Additional file 2: Supplementary Methods). Ammonia nitrogen concentration was quantified using an ammonia nitrogen assay kit (090080, Huankai Biology, Guangzhou, China). Serum samples from HH and LL goats were collected and analyzed for biochemical parameters using an automatic biochemical analyzer (Indiko, Thermo Fisher Scientific, Wilmington, USA).

To construct the GRMGC and goat rumen MAGs database, in addition to the HH ($n = 10$) and LL ($n = 10$) dairy goats, we collected 103 additional goat rumen digesta samples from various breeds via oral gastric tubing. Furthermore, we integrated 37 high-quality rumen digesta metagenomic datasets from 4 published studies [24–27]. In total, 160 samples were available by 7 September 2022. The sample collection comprises seven distinct purebred goat breeds and one hybrid breed, differing in age, sex, housing environment, and feeding regimes: Saanen dairy goats ($n = 100$), Shaanbei white cashmere goats ($n = 8$), Longdong black goats ($n = 7$), Shannan white goats ($n = 8$), Tibetan cashmere goats ($n = 10$), Xiangdong black goats ($n = 6$), Hainan black goats ($n = 9$), and a hybrid population derived from Boer goats (father), and Yangtze Delta white goats (mother) ($n = 12$) (Fig. 1A and Additional file 1: Table S1). All sampling activities were conducted between September and November 2022. For the 6 months preceding sampling, donor goats remained healthy and received no probiotics or antibiotics. All freshly collected rumen digesta samples were immediately stored at − 80 °C prior to total DNA extraction.

To assess the impact of PB14 on milk production performance and rumen fermentation parameters in dairy goats, a total of 10 healthy Guanzhong dairy goats in late lactation (parity = 1, *DIM* = 215.30 ± 3.03 days; mean ± SD) were selected from, and housed at, a farm in Fufeng County, Baoji, Shaanxi province (34°22′N, 107°53′E). The goats were randomly divided into a control group (CON) and a PB14 gavage group (PB), with each group housed in separate well-ventilated pens. The experiment lasted 17 days, during which the average daily minimum and maximum temperatures were 21.71 °C and 31.06 °C, respectively. Both the CON and PB groups of dairy goats underwent an initial 7-day adaptation period followed by a 10-day treatment period. Throughout the entire experiment, goats in both groups had ad libitum access to water, and average feed intake and milk yield were recorded daily. No treatments were administered to either group during

the adaptation period. During the treatment period, the control group (CON) received 20 mL of sterile physiological saline via gavage, while the PB group was administered 20 mL of PB14 suspension (1×10^{11} CFU/L); detailed PB14 suspension preparation methods were provided in the Additional file 2: Supplementary Methods. Milk samples were collected before morning and afternoon milking on the 7th day of the adaptation period and on the 5th and 10th days of the treatment period. The morning and afternoon samples were mixed at a 3:2 (v/v) ratio and analyzed for composition using a FOSS-4000 analyzer (FOSS Electric A/S, Hillerød, Denmark). Rumen fluid was sampled before the first morning feeding (day 1) and 24 h after the final gavage (day 11). Each sample was divided into four aliquots for analysis of VFAs, nicotinate concentrations, and quantification of PB14 [58] and methanogenic archaea [59] copy numbers. Detailed quantification methods were described in the Additional file 2: Supplementary Methods, with primer sequences listed in Additional file 16: Table S15.

Construction and evaluation of the goat rumen microbial gene catalog

DNA was extracted from each sample using the mini-bead beater method described by Yu and Morrison [60]. The extracted DNA was then used for library construction. The newly collected rumen digesta samples in this study consisted of a total of 2.83 Tb of raw metagenomic sequencing data, averaging 23.04 Gb per sample. Additionally, the NCBI-SRA database provided 848.22 Gb of high-quality rumen metagenome data, with an average of 22.92 Gb per sample (Additional file 3: Table S2). Illumina raw sequencing data were processed using fastp [61] (v0.20.0; parameters: –cut_by_quality3 -W 4 -M 20 -n 5 -c -l 50 -w 3) to remove adapters and low-quality reads (length < 50 bp, quality score < 20, and containing N bases). To reduce DNA contamination in the sequencing data, the closest goat genomes, feed ingredient genomes (primarily corresponding to plants included in goat feed), and human genomes were aligned to the raw reads with BWA-MEM [62] (v0.7.17; parameters: -t 20 -M -R "@RG\tID:${sampleid}\tLB:${sampleid}\tPL:UNKNOWN\tSM:${sampleid}"). After quality control and removal of DNA contamination, the 123 rumen digesta samples newly collected here retained 2.25 Tb of high-quality metagenomic sequencing data, averaging 18.32 Gb per sample, while metagenomic datasets from the NCBI-SRA database retained 773.14 Gb of high-quality sequencing data, averaging 20.90 Gb per sample (Additional file 3: Table S2). Subsequently, high-quality sequences from each sample were individually assembled using metaSPAdes [63] (v3.15.5; parameters: –only-assembler -m 400 -t 40). Following assembly, contigs < 500 bp were removed with custom scripts. To optimize sequence utilization and facilitate the identification of rare genes within the goat rumen microbiome, high-quality reads were aligned to their own sample's contigs with Bowtie 2 [64] (v2.5.1; parameters: -p 8) to obtain unassembled reads for each sample. The resulting unmapped reads were pooled and co-assembled with MEGAHIT [65] (v1.2.9; parameters: –min-contig-len 500 -t 40). The individual and joint assemblies yielded

a total of 179,200,950 contigs longer than 500 bp, with an average N50 of 1414.60 bp, an average contig length of 1169.12 bp, and a total length of 202.93×10^{9} bp (Additional file 4: Table S3).

ORFs in the assembled contigs were predicted using Prodigal [66] (v2.6.3; parameters: -p meta), resulting in a total of 304,630,910 ORFs. Complete ORFs accounted for 26.62%, with an average length of 601.16 bp (Additional file 4: Table S3). After removing ORFs shorter than 100 bp, the remaining ORFs were clustered using CD-HIT [67] (v4.8.1; parameters: -n 9 -g 1 -G 0 -m 0 -d 0 -as 0.9 -c 0.95), generating the GRMGC, which contains 73,875,589 NR predicted genes (Additional file 5: Table S4). EMBOSS Transeq [68] (v6.6.0.0; parameters: -frame 6) was employed to translate the representative sequences in the GRMGC into protein sequences for subsequent taxonomic and functional annotation. Gene abundance was determined by aligning the high-quality reads from each sample with NR predicted genes at 95% sequence identity using SOAPaligner/Soap2 [69] (v2.21; parameters: -r 1 -l 35 -M 4 -p 6 -v 20 -c 0.95 -m 400—× 600).

To evaluate the completeness and representativeness of the GRMGC, we clustered the rumen microbial gene catalogs constructed by Xie et al. [26] and Li et al. [28] together with the GRMGC using the large-scale fast clustering tool MMseqs2 [70] (v15.6f452; parameters: easy-linclust –min-seq-id 0.95 -c 0.8 -e 0.001 –threads 40) to remove redundant genes between catalogs. Additionally, we assessed the protein sequence overlap between GRMGC and the rumen microbial NR protein database published by Stewart et al. [29] using MMseqs2 [70]. To evaluate the coverage of GRMGC beyond the cohorts included in this study, rumen microbiome metagenomic sequencing data from three goat studies [4, 30, 31] and two sheep studies [32, 33] were employed. After removing DNA contamination, the external metagenomes were aligned to the GRMGC using BWA-MEM (v0.7.17) [62], and alignment rates were calculated using the "flagstat" function in SAMTOOLS (v1.17) [71].

Taxonomic and functional annotation of NR genes

NR predicted protein sequences were aligned to the NCBI-NR database (October 2022) using DIAMOND [72] (v2.1.8.162) with an *e*-value threshold of ≤ 1e-5 to obtain taxonomic assignments. Predicted proteins without DIAMOND hits were classified as unknown. KOs were assigned to NR predicted proteins with KofamScan [73] (v1.1.0; parameters: –cpu 20 -E 1e-5 -f mapper) by querying the KOfam database with HMMER. KOfam is a customized hidden Markov model (HMM) database for the KOs. In total, 32.12% (23,730,931) of NR predicted proteins mapped to 12,791 KOs and 17.80% (13,151,594) to 464 KEGG level 3 pathways. Functional annotation against eggNOG was performed with eggnog-mapper [74] (v2.1.11; parameters: -d bact, arch, viruses, euk -m diamond –cpu 50 –evalue 1e-5) by aligning the NR predicted protein sequences to the eggNOG 5.0.2 [75] database. A total of 49.44% (36,525,191) of the NR predicted proteins were annotated to 4650 eggNOG orthologous groups. CAZyme annotations were performed using HMMER [76] (v3.3.2) to match protein sequences against the CAZyme family HMM library downloaded from the CAZy database [77] (v.8, http://www.cazy.org/). Overall, 3.88% (2,869,237) of NR predicted proteins were assigned to 637 CAZy families (Additional file 6: Table S5).

Metagenomic binning and genome quality assessment

To deepen the understanding of the goat rumen microbial community, a genomic binning approach was employed. The metaWRAP pipeline [78], comprising multiple functional modules designed for analyzing MAGs, was utilized to reconstruct the goat rumen microbial draft genomes. For contigs assembled from individual samples, the metaWRAP binning module [78] (v1.3.2; parameters: -l 500 –universal –metabat2 –maxbin2 –concoct –interleaved) was applied using three distinct binning algorithms to generate MAGs. For the 160-sample co-assembly, only MetaBAT2 was run [78] (v2.12.1; parameters: -l 1500 –universal –metabat2 –interleaved) to reduce memory demand. Binning of single-sample contigs yielded a total of 115,382 MAGs, while co-assembly binning contributed an additional 2810 MAGs (Additional file 10: Table S9). Subsequently, the metaWRAP bin_refinement module [78] (v 1.3.2; parameters: -t 40 -m 400 -c 50—× 10 –quick) was employed to further refine the assembled MAGs. MAG completeness and contamination were evaluated with CheckM [79] (v1.0.12; parameters: lineage_wf -t 128 -x fa –tab_table). MAGs with completeness greater than 50% and contamination less than 10% were retained. MAGs with completeness between 50 and 90% were classified as medium quality, while those with completeness exceeding 90% and contamination below 5% were designated as high quality [80]. The quality score of each MAG was calculated as completeness − 5 × contamination. Subsequently, dRep [81] (v3.2.2; parameters: -p 72 –ignoreGenomeQuality -pa 0.95 -sa 0.99 -cm larger) was utilized to dereplicate the quality-filtered MAGs at a 99% ANI threshold, resulting in 5514 NR MAGs. These MAGs ranged in size from 0.34 to 9.98 Mb, with N50 lengths ranging from 0.73 to 871.56 kb, an average of 1846 ORFs per MAG, and an average GC% content of 49.82% (Additional file 2: Fig. S24A, B and Additional file 11: Table S10). Similarly, dRep [81] (v3.2.2; parameters: -p 72 –ignoreGenomeQuality -pa 0.90 -sa 0.95 -cm larger) was employed at a 95% ANI threshold to dereplicate the MAGs and identify SGBs. SGBs lacking species-level taxonomy were designated unknown SGBs (uSGBs) [82]. In accordance with the Minimum Information about a Metagenome-Assembled Genome (MIMAG) standards [80] and tRNA and rRNA genes within the 5514 MAGs were identified using tRNAscan-SE [83] (v2.0.12; parameters: -B –thread 20) and Barrnap (v0.9; parameters: –kingdom bac –threads 20 –reject 0.01 –evalue 1e-03; https://github.com/tseemann/barrnap), respectively. The abundance of each MAG within individual samples was assessed using the metaWRAP "quant_bins" [78], where Salmon [84] (v1.9) was utilized to create a reference collection from all MAG contigs. High-quality reads from each sample were then aligned to this reference set to determine the length-weighted average abundance of MAGs within each sample, subsequently represented as TPM values.

Phylogenetic, taxonomic, and functional analyses of MAGs

To elucidate the phylogenetic relationships among the MAGs, ORFs for each MAG were predicted and translated into protein sequences with Prodigal [66] (v2.6.3; parameters: -p single). The resulting MAG-specific protein sequences were processed using PhyloPhlAn [85] (v3.0.67; parameters: -t a -d phylophlan –diversity low –nproc 60)

to generate a maximum likelihood phylogenetic tree, which was subsequently visualized with iTOL [86]. GTDB-tk "classify" [87] (v2.3.0; parameters: –cpus 48 –extension fa –skip_ani_screen) was run to detect bacterial and archaeal marker genes in the 5514 MAGs and assign taxonomy. Detected marker genes were phylogenetically placed against the GTDB r214 reference genome database for precise taxonomic assignment. KOs assignments for all MAG predicted protein sequences were similarly conducted using KofamScan [73]. Subsequently, BLASTP (v2.14.1 +) was utilized to screen protein sequences against the HydDB database, applying an *e*-value cutoff of ≤ 1e-50, coverage greater than 90%, and homology exceeding 50%, to determine the capacity of individual MAG-encoded protein sequences to encode catalytic subunits for three classes of hydrogenases (FeFe –, NiFe –, and Fe –) (Additional file 12: Table S11) [36].

Rumen digesta non-targeted metabolome measurements using LC–MS/MS

For the HH and LL dairy goats, rumen digesta samples frozen at − 80 °C were thawed at 4 °C. Subsequently, 200 μL (± 1 μL) of the thawed sample was aliquoted and combined with 200 μL of internal standard extraction solution (acetonitrile-methanol = 1:4, v/v) and vortexed for 30 s. The resultant mixture was centrifuged at 12,000 rpm for 10 min. Following centrifugation, 200 μL of the supernatant was incubated at − 20 °C for 30 min and subsequently subjected to a second centrifugation at 12,000 rpm under 4 °C for 30 min. Subsequently, 200 μL of the supernatant was transferred to a vacuum concentrator for evaporation and drying. The dried residue was reconstituted in 150 μL of a 70% methanol aqueous solution, vortex-mixed for 3 min, and sonicated in an ice-water bath for 10 min. The mixture was then centrifuged at 12,000 rpm under 4 °C for 3 min, and 120 μL of the supernatant was aliquoted for analysis using a UHPLC-ESI–MS/MS system (UHPLC, ExionLC AD; ESI; QTRAP system).

The UHPLC system was configured with the following conditions: chromatographic column, Waters ACQUITY UPLC HSS T3 C18 (1.8 μm, 2.1 mm × 100 mm); mobile phases, ultrapure water (containing 0.1% formic acid) and acetonitrile (containing 0.1% formic acid); column temperature, 40 °C; flow rate, 0.4 mL/min; and injection volume, 2 μL. MS/MS scans were performed in both positive and negative ionization modes.

The data generated from LC–MS/MS were processed using the Analyst 1.6.3 software package [88]. To expand metabolite identification, metabolites were annotated based on a proprietary MWDB (Metware Database) as well as public databases including Metlin, HMDB, KEGG, and MoNA. Metabolites exhibiting significant differences were identified based on thresholds of $VIP > 1$ and $P < 0.05$. Identified metabolites were initially mapped to KEGG pathways, followed by hypergeometric testing to determine significantly enriched metabolic pathways.

Culture and genomic annotation of rumen-derived P. bryantii B14

The rumen-derived PB14 model strain was acquired from Mingzhou Bio (B260991, Mingzhou Bio, Ningbo, China). PB14 was revived and cultured following DSMZ protocols (https://www.dsmz.de/). The PB14 genome assembly was downloaded from NCBI (https://www.ncbi.nlm.nih.gov/nuccore/NZ_FOEM00000000). CheckM analysis

revealed a genome completeness of 98.1% and contamination of 1.79%, meeting the high-quality draft genome criteria (> 90% completeness, < 5% contamination) as defined by the MIMAG standard [80]. Therefore, this assembly was chosen for downstream analyses. ORFs were predicted with Prodigal (v2.6.3) and translated to protein sequences. KEGG annotation was performed using KofamScan (v1.1.0) with an *e*-value cutoff of ≤ 1e-5 to evaluate the genomic potential of PB14 for nicotinate biosynthesis.

Measurement of P. bryantii B14 growth activity and its synthesis of nicotinate in vitro

PB14 growth was monitored by inoculating the activated culture into M159 and recording OD600 at regular intervals. To evaluate the in vitro nicotinate-producing capacity of PB14, logarithmic-phase cells were enumerated using the plate count technique. Subsequently, 500 μL of PB14 at a concentration of 1×10^8 CFU/mL was inoculated into the PB group ($n = 3$), and 500 μL of heat-inactivated PB14 (100 °C for 10 min) at the same concentration was inoculated into the DPB group ($n = 3$). Cultures were incubated anaerobically at 37 °C within an anaerobic workstation (YQX-III, Chuanhong, Shanghai, China). After incubation, culture supernatants from PB and DPB groups at 0 h and 24 h were harvested by centrifugation at 4000 × *g* for 10 min, and the supernatants were collected for subsequent analyses. Given that the M159 contains nicotinate and its precursor L-aspartate, concentrations of L-aspartate (F0165-OB, FANKEW, Shanghai, China) and nicotinate (F0047-GB, FANKEW, Shanghai, China) in the supernatants of PB and DPB subcultures were quantified using ELISA kits according to the manufacturer's instructions.

Evaluation of P. bryantii B14 impact on methane production in artificial rumen fermentation system

To evaluate the impact of PB14 on methane production, an artificial rumen fermentation system following a previously described protocol [35] with minor modifications was used. Fresh rumen fluid was collected via cannulation before the morning feeding, transferred to anaerobic bags, and incubated at 39.5 °C. All procedures were conducted under continuous CO_2 flow. Each anaerobic bottle received 0.6 g of homogenized, dried total mixed ration. The rumen fluid was mixed with preheated artificial saliva in a 1:4 (v/v) ratio, and 60 mL of this mixture was added to the bottles [89]. In the control group (CON), bottles received 2 mL of sterilized PB14 supernatant filtered through a 0.22-μm membrane. In the PB14 group (PB), bottles were inoculated with 2 mL of active PB14 at 1×10^8 CFU/mL. Following inoculation, bottles were connected to anaerobic gas collection bags equipped with three-way valves and incubated in a shaker (JYCD-202–3, JINWENYIQI, Shanghai, China) at 39.5 °C and 60 rpm for 24 h. Gas volume was measured using a syringe with a three-way valve after fermentation. Methane concentrations were determined using a gas chromatograph (GC-2014C, Shimadzu, Kyoto, Japan) equipped with a TDX-1 column (Agilent Technologies Inc., Santa Clara, USA) according to standard protocols. Total methane production was calculated as gas volume × methane concentration [90]. After fermentation, bottles were placed on ice to halt fermentation, and broth was collected in duplicate for pH measurement and methanogenic archaea

quantification [59]. Detailed methodologies and primer information are provided in the Additional file 2: Supplementary Methods and Additional file 16: Table S15.

Culturing and simulating of bovine mammary epithelial cell line

The MAC-T was cultured in DMEM supplemented with 10% fetal bovine serum under standard conditions of 37 °C and 5% CO_2. Considering that the half-life of NAM in goats is approximately 4 h [40], passaged MAC-T were incubated with NAM at concentrations of 0.0, 0.1, 0.5, 1.0, 2.5, and 5.0 mM for 4 h. Following incubation, the cells were stored at − 80 °C for subsequent qRT-PCR and Western blot analyses. Nonspecific control small interfering RNA (siRNA) and GPR109A-specific siRNA (GenePharma, Shanghai, China) were mixed with Lipofectamine 3000 at a 1:1 (v/v) ratio. The mixture was diluted in serum-free medium and incubated at room temperature for 30 min. Subsequently, the diluted siRNA-Lipofectamine complexes were added to MAC-T in six-well plates and incubated for 24 h to allow transfection. Transfected MAC-T were then seeded into 12-well plates and further incubated with NAM at concentrations of 0.0, 0.1, and 0.5 mM for an additional 4 h. The siRNA sequences used were as follows: 5′-GAACGAGGUUGAUCGAGAAUC-3′.

Quantitative real-time PCR

Total RNA was extracted from MAC-T using the TRIzol reagent (Invitrogen, Carlsbad, CA, USA) following the manufacturer's instructions. The concentration and purity of the extracted RNA were measured using a NanoDrop 2000 spectrophotometer (Thermo Fisher Scientific, Wilmington, USA). RNA integrity was assessed by agarose gel electrophoresis. Subsequently, reverse transcription was performed using the RevertAid First-Strand cDNA Synthesis Kit (Thermo Fisher Scientific, Wilmington, USA) to synthesize cDNA from the total RNA. The qRT-PCR was conducted on a Light Cycler®96 Real-Time PCR System (Roche, Pleasanton, CA) using ChamQ Universal SYBR qPCR Master Mix (Vazyme, Nanjing, China). All primers utilized in this study were designed with Oligo 7 software and preliminarily validated using Primer-BLAST. The primers were synthesized by Zhongke Yutong Biotechnology (Shaanxi, China), and the primer sequences are listed in Additional file 17: Table S16. Relative mRNA expression levels were calculated using the comparative Ct method ($2^{-\Delta\Delta Ct}$).

Western blotting

For MAC-T, an appropriate volume of lysis buffer was added, and the cells were incubated at room temperature for 5 min. The supernatant was subsequently collected for protein analysis through Western blotting. Protein concentrations were determined using the Omni-Easy™ Instant BCA Protein Assay Kit (Epizyme, Shanghai, China) following the manufacturer's instructions. Subsequently, the extracted and quantified protein samples were boiled at 100 °C for 15 min and separated by polyacrylamide gel electrophoresis. Proteins were transferred to a 0.45-μm nitrocellulose membrane using the sandwich transfer method. The membranes were blocked with 5% (w/v) skim milk at room temperature for 1 h. Following blocking, membranes were incubated overnight at 4 °C with the primary antibody. Antibodies against p-S6 (4858S), S6 (no. 2217S), p-ERK (no. 4370), ERK (no. 4695), p-AMPKα (no. 2535), AMPKα (no. 2532), and p-P38 (no. 9211) were obtained from Cell Signaling Technology (MA, USA).

GPR109A (bs-10079R) was obtained from Bioss (Beijing, China). *β*-Actin (mo. 66,009–1-Ig) and P38 (14,064–1-AP) were purchased from Proteintech (Wuhan, China). After primary antibody incubation, membranes were washed 3×5 min with $1 \times$ TBST (T1081, Solarbio, Beijing, China). Subsequently, the membranes were incubated with HRP-conjugated secondary antibodies at room temperature for 1 h. Protein bands were visualized using the Omni-ECL™ Micro Chemiluminescence Kit (Epizyme, Shanghai, China). *β*-Actin was used as the loading control. All blots and gels were derived from the same experiment and processed in parallel.

Statistical analysis

All figures involved in this study were generated in R (v4.3.1) within the RStudio IDE and refined in Adobe Illustrator (v2021). For non-omic data, between-group differences were evaluated with two-tailed unpaired Student's *t-test* (two groups) or one-way ANOVA ($\geq$ three groups). When the ANOVA result was significant, pairwise comparisons were performed with the least significant difference test in SPSS (version 20.0, SPSS, Chicago, IL, USA). Differences were considered statistically significant at $P < 0.05$. Bray–Curtis distance-based ordination analyses were conducted between the HH and LL groups at the species, KOs, KEGG module, and metabolite levels. PERMANOVA and ANOSIM tests with 999 permutations were employed using the vegan package [91] in R to evaluate intergroup differences, followed by PCoA for visualization. The Wilcoxon rank-sum test was utilized to identify significant differences in the relative abundance of various taxa between groups across different taxonomic levels. LEfSe was utilized to compare species-level differences in the rumen microbiota of HH and LL dairy goats. The nonparametric factorial Kruskal–Wallis sum-rank test was used to identify species with significant abundance differences, and the Wilcoxon rank-sum test was applied to assess the consistency of differential species across subgroups between different groups. Subsequently, linear discriminant analysis (LDA) was used to evaluate the impact of each taxon abundance on the differential effect. A significant increase in microbial species abundance was defined as an LDA score $(\log_{10}) > 2.0$ and a $P < 0.05$. LEfSe was also utilized to compare the abundance of microbial metabolic pathways and modules between the two groups, with differences considered statistically significant at LDA scores > 2 and $P < 0.05$. Metabolites with VIP ≥ 1 and $P < 0.05$ were regarded as exhibiting significant differential relative abundance.

Supplementary Information

The online version contains supplementary material available at https://doi.org/10.1186/s13059-025-03788-z.

Additional file 1: Table S1. Background information on 160 goat rumen digesta samples.

Additional file 2: Supplementary Results. Compendium of 5514 de novo microbial genomes from the goat rumen. Hydrogenase profiling of the goat rumen microbiome. Supplementary Methods. Feeding protocol and dietary composition for dairy goats. Determination of volatile fatty acids in goat rumen digesta. DNA extraction, library construction, and metagenomic sequencing. Quantitative real-time PCR analysis of *Prevotella, P. bryantti* B14 and methanogenic archaea. Supplementary Figure: Fig. S1 Metagenomic sequencing data DNA contamination statistics. Fig. S2 Comparison of the GRMGC to the public datasets. Fig. S3 Taxonomic annotation information of NR predicted genes in GRMGC based on the NCBI-NR database. Fig. S4 Comparative analysis of additional lactation phenotypes and rumen fermentation parameters between HH and LL dairy goats. Fig. S5 Comparative analysis of α-diversity in the rumen microbiome between HH and LL dairy goats, assessed using the ACE index (A) and Chao index (B) ($n = 10$/group). Fig S6 Comparative analysis of rumen microbial phyla in HH and LL Dairy goats. Fig. S7 Comparative analysis

of *Prevotella* copy numbers in HH and LL dairy goats. Fig. S8 Comparative analysis of archaeal species in the rumen of HH and LL dairy goats. Fig. S9 Principal coordinate analysis was performed utilizing the Bray-Curtis dissimilarity matrix at the levels of KEGG Orthology (KO) (A), KEGG Module (B), and metabolites (C). Fig. S10 Comparative analysis of KEGG Modules within the rumen microbiome of HH and LL dairy goats. Fig. S11 Pathway enrichment analysis delineating the significant alterations in rumen metabolites between HH and LL dairy goats ($n = 10$/group). Fig. S12 Comparative analysis of microbial enzyme genes (A) and metabolites (B) in the rumen of HH and LL dairy goats ($n = 10$/group). Fig. S13 Thiamine metabolism mediated by the goat rumen microbiome. Fig. S14 Phylogenetic tree of *Prevotella* constructed based on based on MAGs protein sequences. Fig. S15 Growth curve of *P. bryantii* B14. Fig. S16 Effects of *P. bryantii* B14 presence (PB) or absence (CON) on the average daily feed intake of late-lactation dairy goats. Fig. S17 Effects of *P. bryantii* B14 presence (PB) or absence (CON) on the copy numbers of *P. bryantii* B14 (A) and methanogenic archaea (B) in the rumen of late-lactation dairy goats ($n = 5$/group). Fig. S18 Effects of *P. bryantii* B14 presence (PB) or absence (CON) on total VFAs (A), acetate (B), propionate(C), valerate (D), pH (E), butyrate (F), isobutyrate (G), isovalerate (H), and A/P ratio (I) in the rumen of late-lactation dairy goats ($n = 5$/group). Fig. S19 Effects of *P. bryantii* B14 presence (PB) or absence (CON) on nicotinate concentration in the rumen of late-lactation dairy goats ($n = 5$/group). Fig. S20 Effects of varying nicotinamide (NAM) concentrations on the proliferation of bovine mammary epithelial cells (MAC-T). Fig. S21 Assessment of p-AMPK-α, p-ERK, and p-P38 levels in MAC-T treated with a concentration gradient of NAM by western blot, using β-actin as a loading control. Fig. S22 Validate the effect of siGPR109A using qRT-PCR ($n = 3$/group). Fig. S23 Combined inhibition of PKA signaling partially restores mTORC1 activity under GPR109A knockdown. Fig. S24 Quality and taxonomic allocation of MAGs in the rumen of goats. Fig. S25 Phylogenetic tree constructed from 5514 MAGs in the goat rumen. Fig. S26 Phylogenetic tree of hydrogenases from goat rumen MAGs.

Additional file 3: Table S2. Statistical information of the metagenomic sequencing data of goat rumen digesta samples.

Additional file 4: Table S3. Assembly results of the goat rumen digesta samples.

Additional file 5: Table S4. Description of the goat rumen microbial gene catalog (GRMGC).

Additional file 6: Table S5. Number and percentage of the non-redundant (NR) predicted genes in the GRMGC annotated to each item of the various databases.

Additional file 7: Table S6. The top 10 functional capacities of the goat rumen microbiome based on abundance in eggNOG, KEGG, CAZy, CARD, and VFDB databases.

Additional file 8: Table S7. Lactation phenotype of the 177 dairy goats in the research cohort.

Additional file 9: Table S8. Comparative analysis of serum physiological and biochemical parameters in high milk yield, high milk fat content (HH) and low milk yield, low milk fat percentage (LL) dairy goats.

Additional file 10: Table S9. Basic genome binning results statistics.

Additional file 11: Table S10. Statistical summary of 5514 metagenome-assembled genomes (MAGs) from goat rumen.

Additional file 12: Table S11. Statistics description of hydrogenase profiles for 4973 MAGs.

Additional file 13: Table S12. 1017 MAGs showing significant differences between the HH and LL dairy goats.

Additional file 14: Table S13. Differential analysis of premium Prevotella MAGs (Completeness > 80%, Contamination < 10%) between the HH and LL dairy goats.

Additional file 15: Table S14. Feed ingredients and dietary nutrient composition of dairy goats (Dry matter [DM] basis, %).

Additional file 16: Table S15. Primer sequences for qRT-PCR of target microorganism.

Additional file 17: Table S16. Primer sequences used for qRT-PCR analysis of lipid synthesis genes.

Additional file 18: Table S17. Quality assessment and genomic features of species-level genome bins (SGBs) from goat rumen.

Acknowledgements
We appreciate the support from Prof. Qiang Qiu's lab at Northwestern Polytechnical University in conducting the metagenomic analysis. Additionally, we are thankful to Qingdao TongyuanGene Co., LTD for providing the computational resources necessary for this study. We also appreciate the support provided by the Northwest A&F University Gene Editing Scientific Teaching (NWAFU-GEST) platform.

Peer-review information
Andrew Cosgrove was the primary editor of this article and managed its editorial process and peer review in collaboration with the rest of the editorial team. The peer-review history is available in the online version of this article.

Authors' contributions
Conceptualization, Y.L., and K.Z.; methodology, Y.L., Y.N.Z., Y.T.Y., X.M.Z., Y.X.T., Q.Q., Y.L.C., L.D., Z.P.L., X.L.W., and K.Z.; investigation, Y.L., Y.N.Z, Y.T.Y., K.Z., Y.B.X., B.Y., L.G., Z.M.M., X.C., J.P.S., and T.Z.; writing – original, draft, Y.L., Y.N.Z., Y.T.Y., and K.Z.; writing – review and editing, Y.L., L.D., Z.P.L., X.L.W., and K.Z.; funding acquisition, X.L.W., Y.L.C., and K.Z.; resources, S.W.C.; supervision, Y.L.C., Z.P.L., L.D., X.L.W., and K.Z. All authors read and approved the final version of the paper.

Funding
This research was supported by the Biological Breeding–Major Projects (2022ZD04014), the National Key Research and Development Program of China (2022YFD1300203), the National Natural Science Foundation of China (32402785), the China Agricultural Research System (CARS-39–03), and the Key Research and Development Program of Shaanxi Province (2024PT-ZCK-71–3).

Data availability
Raw sequence reads for all samples are available under the NCBI project: PRJNA1162942 [92]. 5514 MAGs along with their ORFs and protein sequences have been deposited in Figshare (https://figshare.com/account/home#/projects/223368) [93]. The source code to generate the gene catalogs, genomic analysis, and functional annotations are available at https://github.com/ylei14/GRMGC [94] and Zenodo (DOI: https://doi.org/10.5281/zenodo.16885342) [95], under a GPL 3.0 license.

Declarations

Ethics approval and consent to participate
All procedures involving animal care and experimental design were approved by the Animal Ethics Committee of Northwest A&F University (Xianyang, Shaanxi, China). All experiments were conducted in accordance with the university's animal research guidelines under License No. 20220923008.

Consent for publication
Not applicable.

Competing interests
Shihwei Chen is employed by Qingyang Weihe Dairy Products Co., Ltd, and all other authors declare no competing interests.

Author details
[1]International Joint Agriculture Research Center for Animal Bio-Breeding, Ministry of Agriculture and Rural Affairs/Key Laboratory of Animal Genetics, Breeding and Reproduction of Shaanxi Province, College of Animal Science and Technology, Northwest A&F University, Yangling 712100, China. [2]College of Animal Science and Technology, Jilin Agricultural University, Changchun 130118, China. [3]Key Laboratory for Agro-Ecological Processes in Subtropical Region, Institute of Subtropical Agriculture, Chinese Academy of Sciences, Changsha 410125, China. [4]School of Ecology and Environment, Northwestern Polytechnical University, Xi'an 710100, China. [5]College of Animal Science and Technology, Gansu Agricultural University, Lanzhou 730070, China. [6]Qingyang Weihe Dairy Products Co., Ltd., Qingyang 745000, China. [7]Key Laboratory of Livestock Biology, Northwest A&F University, Yangling 712100, China. [8]Hainan Institute of Northwest A&F University, Sanya, Hainan 572025, China.

Received: 30 January 2025 Accepted: 14 September 2025
Published online: 26 September 2025

References

1. Herrero M, Thornton PK. Livestock and global change: emerging issues for sustainable food systems. Proc Natl Acad Sci U S A. 2013;110(52):20878–81.
2. Soyeurt H, Dardenne P, Gillon A, Croquet C, Vanderick S, Mayeres P, et al. Variation in fatty acid contents of milk and milk fat within and across breeds. J Dairy Sci. 2006;89(12):4858–65.
3. Bailey KW, Jones CM, Heinrichs AJ. Economic returns to Holstein and Jersey herds under multiple component pricing. J Dairy Sci. 2005;88(6):2269–80.
4. Wang D, Chen L, Tang G, Yu J, Chen J, Li Z, et al. Multi-omics revealed the long-term effect of ruminal keystone bacteria and the microbial metabolome on lactation performance in adult dairy goats. Microbiome. 2023;11(1):215.
5. Chilliard Y, Ferlay A, Rouel J, Lamberet G. A review of nutritional and physiological factors affecting goat milk lipid synthesis and lipolysis. J Dairy Sci. 2003;86(5):1751–70.
6. Zhang M, Liu Z, Wu K, Zhang C, Fu T, Sun Y, et al. The ruminal microbiome alterations associated with diet-induced milk fat depression and milk fat globule size reduction in dairy goats. Animals. 2024;14(17):2614.
7. Zheng L, Wu S, Shen J, Han X, Jin C, Chen X, et al. High rumen degradable starch decreased goat milk fat via *trans*-10, *cis*-12 conjugated linoleic acid-mediated downregulation of lipogenesis genes, particularly, INSIG1. J Anim Sci Biotechnol. 2020;11:1–14.
8. Bergillos-Meca T, Cabrera-Vique C, Artacho R, Moreno-Montoro M, Navarro-Alarcón M, Olalla M, et al. Does *Lactobacillus plantarum* or ultrafiltration process improve Ca, Mg, Zn and P bioavailability from fermented goats' milk? Food Chem. 2015;187:314–21.
9. Kay J, Weber WJ, Moore C, Bauman D, Hansen LB, Chester-Jones H, et al. Effects of week of lactation and genetic selection for milk yield on milk fatty acid composition in Holstein cows. J Dairy Sci. 2005;88(11):3886–93.
10. Stoop W, Van Arendonk J, Heck J, Van Valenberg H, Bovenhuis H. Genetic parameters for major milk fatty acids and milk production traits of Dutch Holstein-friesians. J Dairy Sci. 2008;91(1):385–94.
11. Bauman DE, Griinari JM. Nutritional regulation of milk fat synthesis. Annu Rev Nutr. 2003;23(1):203–27.
12. Marumo J, Lusseau D, Speakman J, Mackie M, Hambly C. Influence of environmental factors and parity on milk yield dynamics in barn-housed dairy cattle. J Dairy Sci. 2022;105(2):1225–41.
13. Baumgard L, Collier RJ, Bauman D. A 100-year review: regulation of nutrient partitioning to support lactation. J Dairy Sci. 2017;100(12):10353–66.

14. Zhang C, Wang M, Liu H, Jiang X, Chen X, Liu T, et al. Multi-omics reveals that the host-microbiome metabolism crosstalk of differential rumen bacterial enterotypes can regulate the milk protein synthesis of dairy cows. J Anim Sci Biotechnol. 2023;14(1):63.
15. Tian H, Niu H, Luo J, Yao W, Chen X, Wu J, et al. Knockout of stearoyl-CoA desaturase 1 decreased milk fat and unsaturated fatty acid contents of the goat model generated by CRISPR/Cas9. J Agric Food Chem. 2022;70(13):4030–43.
16. Xue M-Y, Xie Y-Y, Zhong Y, Ma X-J, Sun H-Z, Liu J-X. Integrated meta-omics reveals new ruminal microbial features associated with feed efficiency in dairy cattle. Microbiome. 2022;10(1):32.
17. Shabat SKB, Sasson G, Doron-Faigenboim A, Durman T, Yaacoby S, Berg Miller ME, et al. Specific microbiome-dependent mechanisms underlie the energy harvest efficiency of ruminants. ISME J. 2016;10(12):2958–72.
18. Urrutia N, Bomberger R, Matamoros C, Harvatine K. Effect of dietary supplementation of sodium acetate and calcium butyrate on milk fat synthesis in lactating dairy cows. J Dairy Sci. 2019;102(6):5172–81.
19. Zhang J, Bu L, Liu Y, Huo W, Xia C, Pei C, et al. Dietary supplementation of sodium butyrate enhances lactation performance by promoting nutrient digestion and mammary gland development in dairy cows. Anim Nutr. 2023;15:137–48.
20. Lemosquet S, Delamaire E, Lapierre H, Blum J, Peyraud J. Effects of glucose, propionic acid, and nonessential amino acids on glucose metabolism and milk yield in Holstein dairy cows. J Dairy Sci. 2009;92(7):3244–57.
21. Moraïs S, Mizrahi I. The road not taken: the rumen microbiome, functional groups, and community states. Trends Microbiol. 2019;27(6):538–49.
22. Xue M-Y, Sun H-Z, Wu X-H, Liu J-X, Guan LL. Multi-omics reveals that the rumen microbiome and its metabolome together with the host metabolome contribute to individualized dairy cow performance. Microbiome. 2020;8:1–19.
23. Zhang C, Liu H, Jiang X, Zhang Z, Hou X, Wang Y, et al. An integrated microbiome-and metabolome-genome-wide association study reveals the role of heritable ruminal microbial carbohydrate metabolism in lactation performance in Holstein dairy cows. Microbiome. 2024;12:232.
24. Lu Z, Xu Z, Kong L, Shen H, Aschenbach JR. Functional changes of the community of microbes with Ni-dependent enzyme genes accompany adaptation of the ruminal microbiome to urea-supplemented diets. Front Microbiol. 2020;11:596681.
25. Zhang T, Li M, Shi T, Yan Y, Niyazbekova Z, Wang X, et al. Transmission of the gut microbiome in cohousing goats and pigs. Front Microbiol. 2022;13:948617.
26. Xie F, Jin W, Si H, Yuan Y, Tao Y, Liu J, et al. An integrated gene catalog and over 10,000 metagenome-assembled genomes from the gastrointestinal microbiome of ruminants. Microbiome. 2021;9(1):137.
27. Zhang K, He C, Xu Y, Zhang C, Li C, Jing X, et al. Taxonomic and functional adaption of the gastrointestinal microbiome of goats kept at high altitude (4800 m) under intensive or extensive rearing conditions. FEMS Microbiol Ecol. 2021;97(3):fiab009.
28. Li J, Zhong H, Ramayo-Caldas Y, Terrapon N, Lombard V, Potocki-Veronese G, et al. A catalog of microbial genes from the bovine rumen unveils a specialized and diverse biomass-degrading environment. Gigascience. 2020;9(6):giaa057.
29. Stewart RD, Auffret MD, Warr A, Walker AW, Roehe R, Watson M. Compendium of 4,941 rumen metagenome-assembled genomes for rumen microbiome biology and enzyme discovery. Nat Biotechnol. 2019;37(8):953–61.
30. Cao Y, Feng T, Wu Y, Xu Y, Du L, Wang T, et al. The multi-kingdom microbiome of the goat gastrointestinal tract. Microbiome. 2023;11(1):219.
31. Shen J, Zheng L, Chen X, Han X, Cao Y, Yao J. Metagenomic analyses of microbial and carbohydrate-active enzymes in the rumen of dairy goats fed different rumen degradable starch. Front Microbiol. 2020;11:1003.
32. Li Z, Shen J, Xu Y, Zhu W. Metagenomic analysis reveals significant differences in microbiome and metabolic profiles in the rumen of sheep fed low N diet with increased urea supplementation. FEMS Microbiol Ecol. 2020;96(10):fiaa117.
33. Xue Y, Lin L, Hu F, Zhu W, Mao S. Disruption of ruminal homeostasis by malnutrition involved in systemic ruminal microbiota-host interactions in a pregnant sheep model. Microbiome. 2020;8(1):138.
34. Moya A, Ferrer M. Functional redundancy-induced stability of gut microbiota subjected to disturbance. Trends Microbiol. 2016;24(5):402–13.
35. Li Q, Ma Z, Huo J, Zhang X, Wang R, Zhang S, et al. Distinct microbial hydrogen and reductant disposal pathways explain interbreed variations in ruminant methane yield. ISME J. 2024. https://doi.org/10.1093/ismejo/wrad016.
36. Greening C, Geier R, Wang C, Woods LC, Morales SE, McDonald MJ, et al. Diverse hydrogen production and consumption pathways influence methane production in ruminants. ISME J. 2019;13(10):2617–32.
37. Lin L, Lai Z, Zhang J, Zhu W, Mao S. The gastrointestinal microbiome in dairy cattle is constrained by the deterministic driver of the region and the modified effect of diet. Microbiome. 2023;11(1):10.
38. Lin L, Lai Z, Yang H, Zhang J, Qi W, Xie F, et al. Genome-centric investigation of bile acid metabolizing microbiota of dairy cows and associated diet-induced functional implications. ISME J. 2023;17(1):172–84.
39. Nohr D, Biesalski H. Vitamins in milk and dairy products: B-group vitamins. Advanced Dairy Chemistry: Volume 3: Lactose, Water, Salts and Minor Constituents. 2009:591–630.
40. Chen J, Yang Z, Dong G. Niacin nutrition and rumen-protected niacin supplementation in dairy cows: an updated review. Br J Nutr. 2019;122(10):1103–12.
41. Guo W, Liu J, Li W, Ma H, Gong Q, Kan X, et al. Niacin alleviates dairy cow mastitis by regulating the GPR109A/AMPK/NRF2 signaling pathway. Int J Mol Sci. 2020;21(9):3321.
42. Lapidus AL, Korobeynikov AI. Metagenomic data assembly–the way of decoding unknown microorganisms. Front Microbiol. 2021;12:613791.
43. Zhang Y, Zheng Y, Wang X, Qiu J, Liang C, Cheng G, et al. Bovine stearoyl-CoA desaturase 1 promotes adipogenesis by activating the PPARγ receptor. J Agric Food Chem. 2020;68(43):12058–66.
44. Ahmed K, Tunaru S, Offermanns S. GPR109A, GPR109B and GPR81, a family of hydroxy-carboxylic acid receptors. Trends Pharmacol Sci. 2009;30(11):557–62.
45. Wu Z, Tian M, Heng J, Chen J, Chen F, Guan W, et al. Current evidences and future perspectives for AMPK in the regulation of milk production and mammary gland biology. Front Cell Dev Biol. 2020;8:530.

46. Fan L, Xia Y, Wang Y, Han D, Liu Y, Li J, et al. Gut microbiota bridges dietary nutrients and host immunity. Sci China Life Sci. 2023;66(11):2466–514.
47. Clark AJ, Parikh SM. Targeting energy pathways in kidney disease: the roles of sirtuins, AMPK, and PGC1α. Kidney Int. 2021;99(4):828–40.
48. Shaw RJ. LKB1 and AMP-activated protein kinase control of mTOR signalling and growth. Acta Physiol. 2009;196(1):65–80.
49. Nakagawa-Nagahama Y, Igarashi M, Miura M, Kashiwabara K, Yaku K, Fukamizu Y, et al. Blood levels of nicotinic acid negatively correlate with hearing ability in healthy older men. BMC Geriatr. 2023;23(1):97.
50. Stratford M, Rojas A, Hall D, Dennis M, Dische S, Joiner M, et al. Pharmacokinetics of nicotinamide and its effect on blood pressure, pulse and body temperature in normal human volunteers. Radiother Oncol. 1992;25(1):37–42.
51. Dragovic J, Kim SH, Brown SL, Kim JH. Nicotinamide pharmacokinetics in patients. Radiother Oncol. 1995;36(3):225–8.
52. Souza V, Moraes L, Baumgard L, Santos J, Mueller N, Rhoads R, et al. Modeling the effects of heat stress in animal performance and enteric methane emissions in lactating dairy cows. J Dairy Sci. 2023;106(7):4725–37.
53. Sehested J, Gaillard C, Lehmann J, Maciel G, Vestergaard M, Weisbjerg M, et al. Extended lactation in dairy cattle. Animal. 2019;13(S1):s65–74.
54. Guo L, Xi B, Lu L. Strategies to enhance production of metabolites in microbial co-culture systems. Bioresour Technol. 2024. https://doi.org/10.1016/j.biortech.2024.131049.
55. Wu X, Sun H, Xue M, Wang D, Liu J. Serum metabolome profiling revealed potential biomarkers for milk protein yield in dairy cows. J Proteomics. 2018;184:54–61.
56. Faul F, Erdfelder E, Buchner A, Lang A-G. Statistical power analyses using G* power 3.1: tests for correlation and regression analyses. Behav Res Methods. 2009;41(4):1149–60.
57. Li X, Yu C, Zhang B, Shan X, Mao W, Zhang Z, et al. The recovery of the microbial community after plaque removal depends on periodontal health status. NPJ Biofilms Microbiomes. 2023;9(1):75.
58. Niu W, He Y, Wang H, Xia C, Shi H, Cao B, et al. Effects of *leymus chinensis* replacement with whole-crop wheat hay on blood parameters, fatty acid composition, and microbiomes of Holstein bulls. J Dairy Sci. 2018;101(1):246–56.
59. Bayat A, Kairenius P, Stefański T, Leskinen H, Comtet-Marre S, Forano E, et al. Effect of camelina oil or live yeasts (*Saccharomyces cerevisiae*) on ruminal methane production, rumen fermentation, and milk fatty acid composition in lactating cows fed grass silage diets. J Dairy Sci. 2015;98(5):3166–81.
60. Yu Z, Morrison M. Improved extraction of PCR-quality community DNA from digesta and fecal samples. Biotechniques. 2004;36(5):808–12.
61. Chen S, Zhou Y, Chen Y, Gu J. Fastp: an ultra-fast all-in-one FASTQ preprocessor. Bioinformatics. 2018;34(17):i884–90.
62. Li H, Durbin R. Fast and accurate long-read alignment with Burrows-Wheeler transform. Bioinformatics. 2010;26(5):589–95.
63. Nurk S, Meleshko D, Korobeynikov A, Pevzner PA. Metaspades: a new versatile metagenomic assembler. Genome Res. 2017;27(5):824–34.
64. Langmead B, Salzberg SL. Fast gapped-read alignment with bowtie 2. Nat Methods. 2012;9(4):357–9.
65. Li D, Liu C-M, Luo R, Sadakane K, Lam T-W. MEGAHIT: an ultra-fast single-node solution for large and complex metagenomics assembly via succinct de Bruijn graph. Bioinformatics. 2015;31(10):1674–6.
66. Hyatt D, Chen G-L, LoCascio PF, Land ML, Larimer FW, Hauser LJ. Prodigal: prokaryotic gene recognition and translation initiation site identification. BMC Bioinformatics. 2010;11:1–11.
67. Fu L, Niu B, Zhu Z, Wu S, Li W. CD-hit: accelerated for clustering the next-generation sequencing data. Bioinformatics. 2012;28(23):3150–2.
68. Madeira F, Park YM, Lee J, Buso N, Gur T, Madhusoodanan N, et al. The EMBL-EBI search and sequence analysis tools APIs in 2019. Nucleic Acids Res. 2019;47(W1):W636–41.
69. Li R, Yu C, Li Y, Lam T-W, Yiu S-M, Kristiansen K, et al. SOAP2: an improved ultrafast tool for short read alignment. Bioinformatics. 2009;25(15):1966–7.
70. Steinegger M, Söding J. MMseqs2 enables sensitive protein sequence searching for the analysis of massive data sets. Nat Biotechnol. 2017;35(11):1026–8.
71. Li H, Handsaker B, Wysoker A, Fennell T, Ruan J, Homer N, et al. The sequence alignment/map format and SAMtools. Bioinformatics. 2009;25(16):2078–9.
72. Buchfink B, Xie C, Huson DH. Fast and sensitive protein alignment using DIAMOND. Nat Methods. 2015;12(1):59–60.
73. Aramaki T, Blanc-Mathieu R, Endo H, Ohkubo K, Kanehisa M, Goto S, et al. KofamKOALA: kegg ortholog assignment based on profile HMM and adaptive score threshold. Bioinformatics. 2020;36(7):2251–2.
74. Huerta-Cepas J, Forslund K, Coelho LP, Szklarczyk D, Jensen LJ, Von Mering C, et al. Fast genome-wide functional annotation through orthology assignment by eggNOG-mapper. Mol Biol Evol. 2017;34(8):2115–22.
75. Huerta-Cepas J, Szklarczyk D, Heller D, Hernández-Plaza A, Forslund SK, Cook H, et al. eggNOG 5.0: a hierarchical, functionally and phylogenetically annotated orthology resource based on 5090 organisms and 2502 viruses. Nucleic Acids Res. 2019;47(D1):D309–14.
76. Potter SC, Luciani A, Eddy SR, Park Y, Lopez R, Finn RD. HMMER web server: 2018 update. Nucleic Acids Res. 2018;46(W1):W200–4.
77. Lombard V, Golaconda Ramulu H, Drula E, Coutinho PM, Henrissat B. The carbohydrate-active enzymes database (CAZy) in 2013. Nucleic Acids Res. 2014;42(D1):D490-5.
78. Uritskiy GV, DiRuggiero J, Taylor J. MetaWRAP—a flexible pipeline for genome-resolved metagenomic data analysis. Microbiome. 2018;6:1–13.
79. Parks DH, Imelfort M, Skennerton CT, Hugenholtz P, Tyson GW. Checkm: assessing the quality of microbial genomes recovered from isolates, single cells, and metagenomes. Genome Res. 2015;25(7):1043–55.
80. Bowers RM, Kyrpides NC, Stepanauskas R, Harmon-Smith M, Doud D, Reddy T, et al. Minimum information about a single amplified genome (MISAG) and a metagenome-assembled genome (MIMAG) of bacteria and archaea. Nat Biotechnol. 2017;35(8):725–31.
81. Olm MR, Brown CT, Brooks B, Banfield JF. dRep: a tool for fast and accurate genomic comparisons that enables improved genome recovery from metagenomes through de-replication. ISME J. 2017;11(12):2864–8.

82. Pasolli E, Asnicar F, Manara S, Zolfo M, Karcher N, Armanini F, et al. Extensive unexplored human microbiome diversity revealed by over 150,000 genomes from metagenomes spanning age, geography, and lifestyle. Cell. 2019;176(3):649–62. e20.
83. Chan PP, Lin BY, Mak AJ, Lowe TM. tRNAscan-SE 2.0: improved detection and functional classification of transfer RNA genes. Nucleic Acids Res. 2021;49(16):9077–96.
84. Patro R, Duggal G, Love MI, Irizarry RA, Kingsford C. Salmon provides fast and bias-aware quantification of transcript expression. Nat Methods. 2017;14(4):417–9.
85. Asnicar F, Thomas AM, Beghini F, Mengoni C, Manara S, Manghi P, et al. Precise phylogenetic analysis of microbial isolates and genomes from metagenomes using PhyloPhlAn 3.0. Nat Commun. 2020;11(1):2500.
86. Letunic I, Bork P. Interactive tree of life (iTOL) v5: an online tool for phylogenetic tree display and annotation. Nucleic Acids Res. 2021;49(W1):W293-6.
87. Chaumeil P-A, Mussig AJ, Hugenholtz P, Parks DH. GTDB-Tk v2: memory friendly classification with the genome taxonomy database. Bioinformatics. 2022;38(23):5315–6.
88. Zhang K, Xu Y, Zheng Y, Zhang T, Wu Y, Yan Y, et al. *Bifidobacterium pseudolongum*-derived bile acid from dietary carvacrol and thymol supplementation attenuates colitis via cGMP-PKG-mTORC1 pathway. Adv Sci. 2024. https://doi.org/10.1002/advs.202406917.
89. Menke K, Raab L, Salewski A, Steingass H, Fritz D, Schneider W. The estimation of the digestibility and metabolizable energy content of ruminant feedingstuffs from the gas production when they are incubated with rumen liquor *in vitro*. J Agric Sci. 1979;93(1):217–22.
90. Navarro-Villa A, O'brien M, López S, Boland T, O'kiely P. Modifications of a gas production technique for assessing in vitro rumen methane production from feedstuffs. Anim Feed Sci Technol. 2011;166:163–74.
91. Dixon P. VEGAN, a package of R functions for community ecology. J Veg Sci. 2003;14(6):927–30.
92. Lei Y, Zheng Y, Yan Y, Zhang K, Sun X, Yang B, et al. Deciphering functional landscapes of rumen microbiota unveils the role of Prevotella bryantii in milk fat synthesis in goats. Datasets. Sequence Read Archive. 2025. https://www.ncbi.nlm.nih.gov/sra?linkname=bioproject_sra_all&from_uid=1162942.
93. Lei Y, Zheng Y, Yan Y, Zhang K, Sun X, Yang B, et al. Deciphering functional landscapes of rumen microbiota unveils the role of Prevotella bryantii in milk fat synthesis in goats. Datasets. Figshare. 2025. https://figshare.com/account/home#/projects/223368.
94. Lei Y, Zheng Y, Yan Y, Zhang K, Sun X, Yang B, et al. Deciphering functional landscapes of rumen microbiota unveils the role of Prevotella bryantii in milk fat synthesis in goats. Github. 2025. https://github.com/ylei14/GRMGC.
95. Lei Y, Zheng Y, Yan Y, Zhang K, Sun X, Yang B, et al. Deciphering functional landscapes of rumen microbiota unveils the role of Prevotella bryantii in milk fat synthesis in goats. 2025. Zenodo. https://doi.org/10.5281/zenodo.16885342.

Publisher's Note